On the Spectral Efficiency of LoRa Networks: Performance Analysis, Trends and Optimal Points of Operation

Lam-Thanh Tu, Abbas Bradai, *Senior Member, IEEE*, Yannis Pousset, and Alexis I. Aravanis

***Abstract*— In the present paper a closed-form framework is derived for the analysis and optimization of the coverage probability (Pcov) and of the area spectral efficiency (ASE) in long-range (LoRa) networks. The proposed framework exploits stochastic geometry tools to associate the Pcov and the ASE to the end device (ED) transmit power and to the ED density. The analysis reveals the trends of the Pcov and of the ASE curves, with respect to both of the two parameters, while the robustness of the framework holds even at the asymptotic cases. Building upon the derived framework, the analysis demonstrates that no joint global optimum exists that jointly maximizes the Pcov over both parameters, suggesting that the optimization of the Pcov must be performed separately, for the two key network parameters considered. As opposed to that, the analysis demonstrates that a set of global optima exists that jointly maximize the ASE over both parameters, and these global maxima are subsequently derived in closed form. Thus, the derived framework fully characterizes the performance of LoRa networks, while defining in closed form the optimal points of operation that can be proven of significant value, for the transceiver and network design, of practical LoRa networks.**

***Index Terms*— LPWAN, LoRa networks, stochastic geometry, system-level analysis, spectral efficiency.**

I. Introduction

THE emerging technology of low power wide area networks (LPWANs) has arisen as a prime candidate for supporting the interconnection of massive number of internet-of-things (IoT) devices, that are characterized by different quality-of-service (QoS) objectives. Among all available LPWAN technologies such as long-range (LoRa), Sigfox and Narrowband-IoT (NB-IoT), LoRa has received an increasing attention both from the industrial and the academic research communities and is widely regarded as the most promising technology toward realizing the LPWAN objectives [2]. The main driving force behind LoRa's success is its patented chirp spread spectrum (CSS) modulation, which outperforms significantly the conventional modulation schemes, like QAM and PSK, with respect to the suppression of noise and fading [3]. Moreover, LoRa can support a wide range of IoT devices and applications, that belong to different QoS tiers, through the appropriate adjustment of its intrinsic parameters, such as the spreading factor (SF), the coding rate (CR) and the bandwidth (BW). In addition, LoRa obviates the need for sensing the medium's availability or for applying any procedure to access the medium thanks to the ALOHA protocol. This allows for the reduction of the ED energy consumption, and allows for the EDs to actively access the medium regardless of the channel occupancy, while the resulting increased interference (compared to other protocols) can be combated at the receiver, due to the intrinsic LoRa characteristics as will be demonstrated in the following sections. Due to these features, LoRa allows for optimizing the overall network performance, and for devising optimization strategies tailored to the network in hand. The development of such strategies, however, is preconditioned on the system-level analysis of the LoRa network, and on the understanding of the performance trends that govern its operation.

In the direction of performing such system-level analysis of LoRa networks, stochastic geometry (SG) can be employed in order to model the random deployment of EDs and gateways, by employing a tractable mathematical framework. The employment of SG for the study of LoRa networks was first performed by Orestis *et al.* in [4], where the deployment of EDs was modelled by a homogeneous Poisson point process (PPP). In their work, however, the correlation, at the receiver, between the signal-to-noise ratio (SNR) and the signal-to-interference-ratio (SIR) is ignored. In [5], the EDs are distributed according to the Matern cluster process and the study focuses on the coverage probability (Pcov) and the area spectral efficiency (ASE) of the network. The employment of the Matern cluster point process allows for capturing more accurately the characteristics of the ED deployments in LoRa networks, however, it introduces a significant intractability in the mathematical framework. In particular, it imposes the

Manuscript received July 26, 2021; revised November 25, 2021; accepted January 24, 2022. Date of publication February 2, 2022; date of current version April 18, 2022. This work was supported in part by the CPER/FEDER NUMERIC project "Intelligent Networks II" under grant agreement NUMERI06 and the H2020 MSCA IF Pathfinder project under grant agreement 891030. An earlier version of this paper was presented in part at the IEEE International Conference on Communications 2020 [1] [DOI: 10.1109/ICC40277.2020.9148720]. The associate editor coordinating the review of this article and approving it for publication was Prof. S. Affes. *(Corresponding author: Lam-Thanh Tu.)*

Lam-Thanh Tu, Abbas Bradai, and Yannis Pousset are with the XLIM Research Institute, University of Poitiers, 86073 Poitiers, France (e-mail: lam.thanh.tu@univ-poitiers.fr; abbas.bradai@univ-poitiers.fr; yannis.pousset@univ-poitiers.fr).

Alexis I. Aravanis is with the Laboratory of Signals and Systems (L2S), Centre National de la Recherche Scientifique (CNRS), CentraleSupélec, University of Paris-Saclay, 91192 Gif-sur-Yvette, France (e-mail: alexis.aravanis@centralesupelec.fr).

Color versions of one or more figures in this article are available at https://doi.org/10.1109/TCOMM.2022.3148784.

Digital Object Identifier 10.1109/TCOMM.2022.3148784

employment of numerical techniques for the computation of the system metrics, which does not allow for understanding the system trends and for obtaining insights into the network behaviour. Hoeller *et al.* studied the performance of LoRa networks for gateways that employ multiple antennas [6]. They, however, also ignore the correlation between the SNR and the SIR at the receiver.

In [7], the Pcov is computed considering either the aggregate interference of all EDs or the interference arising only by the dominant interferer. In spite of the employment of a tractable PPP for the modelling of the ED distribution and of the dominant interferer approximation, the Pcov, still, cannot be derived in a closed form. Therefore, numerical computations are employed instead. However, their findings demonstrated that the Pcov derived by taking into account only the dominant intra-SF interferer constitutes a very accurate approximation of the exact Pcov that is derived by taking into account the aggregate intra-SF interference. In [8], the coverage probability and the energy efficiency in LoRa networks is compared for different MAC protocols, i.e., pure ALOHA, slotted ALOHA and CSMA. The results demonstrate that the slotted ALOHA achieves the highest performance among all considered protocols. However, the analysis also assumes that the SNR and the SIR are independent at the receiver. Experimental results in [9] also revealed that the slotted ALOHA protocol improves significantly the energy efficiency of LoRa network. In [10], the authors developed a framework based on tools from SG for analysing the energy efficiency of LoRa networks, by taking into account the energy consumption at each operating state of the EDs. These states included among others the wake up, sleep, and waiting states.

The performance of LoRa networks has also been investigated under different frameworks, that do not employ SG for the modelling of the ED deployment. In [11], Reynders *et al.* proposed a novel SF allocation scheme, to guarantee a fair collision probability among all SFs. The proposed scheme outperforms the conventional distance-based allocation scheme with respect to the packet error rate, while an extension to this scheme was introduced in [12]. In [13] the authors study the resource allocation problem for LoRa networks with respect to the energy efficiency, introducing a joint power and channel allocation scheme. The end-to-end (e2e) latency of LoRa transmissions is then examined in [14], with the study showing that the e2e latency in LoRa networks can be reduced though the appropriate reduction of the arrival rate.

Building upon the aforementioned works, the present paper, studies the system-level performance of LoRa networks employing a PPP for modelling the distribution of the EDs, while assuming that the small-scale fading follows a Nakagami-m distribution (that incorporates many fading distributions including Rayleigh). As opposed to [4], [6], [8] the introduced framework takes into account the correlation between the SNR and the SIR at the receiver. Moreover, as opposed to [5], [7] where the Pcov and the ASE were computed through numerical computations, the present paper derives approximate, albeit accurate, closed-form expressions for both metrics. This allows for gaining insights into the performance trends of the network by associating the Pcov and the ASE to fundamental network and ED design parameters, namely the ED density and the ED transmit power. This allows for the optimal transceiver design and the optimization of the LoRa network parameters, with respect to the maximization of the Pcov and the ASE. More precisely, the main contributions of the present paper can be outlined as follows:

- A novel formulation of the coverage probability is introduced, that takes into account the correlation between the SIR and the SNR at the receiver. Building upon this definition, we derive approximate, albeit tight, closed-form expressions for both the Pcov and the ASE.
- The derived closed-form framework provides insights into the behavior of Pcov with respect to key network parameters, namely, the ED density and the transmit power. In particular, Pcov is demonstrated to be a monotonically decreasing convex function with respect to the density of EDs and a concave, monotonically increasing function with respect to the transmit power. Pcov is also computed for the asymptotic cases where the ED density and the transmit power tend to infinity and zero respectively. The introduced Pcov approximation is also compared, via numerical simulations, against the pervasive Pcov approximation that ignores the correlation between the SNR and the SIR at the receiver, demonstrating the superior performance of the introduced approximation with respect to the accuracy of the results.
- Subsequently, focusing on the ASE, the derived closed-form framework provides insights into the behavior of the ASE with respect to the density of EDs and the transmit power. It is demonstrated that the ASE has an identical behavior with Pcov with respect to the transmit power, while the trends of the ASE with respect to the density of EDs is more complex than that of the Pcov. In particular, the ASE is either a concave function that increases monotonically with the ED density or is a unimodal function of the ED density.
- The trade-off between the path-loss exponent and the optimal density of EDs is examined.
- Subsequently, the trends of the Pcov and of the ASE are studied jointly, taking into account the impact of both the transmit power and the ED density in the analysis. It is, thus, evinced that no pair of ED transmit power and ED density exists that jointly maximizes the Pcov, and that the optimization with respect to Pcov needs to be therefore performed individually for each of the two terms. However, it is proven that a set of pairs of ED transmit power and ED density exists that jointly maximize the ASE, that is the figure of merit quantifying the overall network performance. The set of optimum pairs maximizing the ASE is derived in closed form, thus allowing for the optimal transceiver design (with respect to transmit power) and the optimization of the LoRa network deployment (with respect to the ED density).
- Numerical results are also provided to corroborate the accuracy of the derived mathematical framework, while the introduced approach considering only the dominant intra-SF interferer is shown to serve as a tight upper

bound for the case where the sum of the aggregate (both intra-SF and inter-SF) interference is taken into account.

Compared to the conference version, we have added the following contributions:

- We have considered two spreading factor allocations, namely, the fair-collision and the random SF allocations as opposed to only the random allocation.
- We have examined the behavior of the Pcov and of the ASE with respect to both the transmit power and the density of EDs simultaneously.
- We have derived the joint optimums of the ASE in closed form, maximizing the ASE over both the transmit power and the density of EDs.
- We have provided full derivations of all Propositions and Theorems.
- We have provided a thorough justification for all considered approximations.
- We have employed the exact framework for the packet length.
- We have derived in closed form the inflection point of the ASE with respect to the average number of EDs.
- We have investigated the trends of the optimum and of the inflection point of the ASE with respect to the path-loss exponent.
- We have produced new figures and more numerical results (based on the aggregate interference (both co-SF and inter-SF interference) accounting also for the case where the SIR and the SNR are considered to be independent). These numerical results are then compared with our approximate framework that does not assume (for simplicity) the SNR and SIR to be independent demonstrating the superior performance of the latter.

The remainder of the paper is organized as follows. Section II, introduces the system model. Section III, presents the framework for the analysis of the Pcov and of the ASE. Subsequently the trends and behaviors of those metrics are investigated in Section IV. Section V, presents the Monte Carlo simulations corroborating the accuracy of the proposed framework. Finally, Section VI concludes the paper and presents perspectives.

II. System Model

A. LoRa Networks Modeling

Let us consider an uplink LoRa network comprising a gateway located at the center of a disc of radius R and a set of EDs randomly deployed within the area of the disc according to the inhomogeneous PPP Ψ. The intensity function is $\lambda = \overline{N}/\mathcal{Q} > 0$ where $\overline{N}$ is the average number of EDs in the area of the disc and $\mathcal{Q} = \pi R^2$ is the area of the disc (i.e. the area of the considered network). The interference from different technologies that may operate at the same industrial, scientific or medical (ISM) band is not considered, as is typically the case in the literature [4], [6], [7].

B. Channel Modelling

The signals transmitted by the EDs to the gateway are subjected to both small-scale fading and large-scale path-loss. The impact of the shadowing is not taken into account, as its effects can be simply incorporated into the analysis by appropriately scaling the value of λ [18].

1) Small-Scale Fading: The small-scale fading from an arbitrary node o to the gateway is denoted by h_o and h_o is assumed to follow a Nakagami-m distribution with shape and spread parameters $m \geq 1/2$ and Ω, respectively. As a result, the channel gain h_o^2 follows a Gamma distribution of shape and scale parameters m and $\theta = \Omega/m$, respectively. The Nakagami-m fading is considered for the analysis, since it constitutes a general case of fading that can represent a wide range of fading distributions through the appropriate adjustment of the shape parameters. For instance, for $m = 1$ the fading follows a Rayleigh distribution and for $m = 1/2$ it follows the single-sided Gaussian distribution.

2) Large-Scale Path-Loss: Focusing on the transmission link from a generic node o to the gateway, then the large-scale path-loss of the link is given by [10]

$$L_o = l\left(r_o\right) = K_0 r_o^{\beta}, \tag{1}$$

where r_o is the distance from the ED o to the gateway. Moreover, $\beta > 2$ is the path-loss exponent and $K_0 = \left(\frac{4\pi f_c}{c}\right)^2$ is the path-loss constant. f_c is the carrier frequency and $c = 3 \times 10^8$ (in meters per second) is the speed of light.

C. Spreading Factor Allocation

1) Fair-Collision Scheme: The SF allocation scheme adopted herein is the one proposed in [11], that guarantees a fair collision probability among all available SFs. This scheme has been chosen since it improves the network performance significantly compared to the popular distance-based allocation scheme [11], [12]. Under this scheme, the probability that an ED is assigned the SF k is given by

$$p_k^{\text{fa}} = (k/2^k)/\sum\nolimits_{i=7}^{12}(i/2^i), \quad k \in \{7, \ldots, 12\}. \tag{2}$$

Hence, the density of EDs of SF k under the fair-collision scheme is given by $\lambda_k^{\text{fa}} = p_k^{\text{fa}}\lambda$.

2) Random Scheme: Alternatively, under a random assignment regime, each ED can be randomly assigned an arbitrary SF by the gateway and the probability that an ED is assigned the SF k is $p_k^{\text{ra}} = 1/6, \forall k$ while the density of EDs of SFk is then given by $\lambda_k^{\text{ra}} = p_k^{\text{ra}}\lambda = \lambda/6$.

D. Interference Modeling

In LoRa, the number of concurrent transmissions is limited due to the strict constraints on the duty cycle. However, even in the case of concurrent transmissions the receiver can still decode correctly the transmitted symbol, provided that (a) the received signal strength from the intended ED is higher than that from an interfering ED that transmits using the same SF [1] and (b) that the intended ED and the interfering ED using the same SF do not transmit the same symbol simultaneously [8]. However, the probability of having

[1] In practice though, the adopted co-SF interference thresholds can vary greatly.

TABLE I
MAIN NOTATIONS AND MATHEMATICAL SYMBOLS

Symbol	Definition
$\mathbb{E}\{.\}$, $\Pr(.)$	Expectation and probability operators
$\Gamma(.)$, $\gamma(.,.)$	Gamma and lower incomplete gamma functions
$\exp(.)$, $\ln(.)$	Exponential and logarithm functions
$F_X(x)$	Cumulative distribution function (CDF) of RV X
$f_X(x)$	Probability density function (PDF) of RV X
$\mathbf{1}(x)$,	Indicator function
$\dot{f}(x) = df(x)/dx$	First-order derivative of f with respect to x
$\ddot{f}(x) = d^2 f(x)/dx^2$	Second-order derivative of f with respect to x
$\max\{.\}$	Maximum function
$\text{Pcov}(\gamma_{\text{D},k}, s)$	Exact Pcov of SF k and s SF allocation scheme
$\widetilde{\text{Pcov}}(\gamma_{\text{D},k}, s)$	Approximated Pcov of SF k and s SF allocation scheme
ASE_s, $\widetilde{\text{ASE}}_s$	Exact and Approximated ASE of s SF allocation scheme
Det $\{X\}$	The determinant of the X matrix
$H(x,y)$	The Hessian matrix of variables x and y
λ_k, $\overline{N}_k$	The density and average number of EDs of SF k
β, K_0	The path-loss exponent and path-loss constant
P_{tx}, σ^2	The transmit power and noise variance

the same symbol being transmitted simultaneously by two messages is, for instance, for a SF7 and a SF12 around 3% and 0.1%, respectively. Moreover, regardless of the signal strength, the receiver can still correctly decode the signal, as long as at least five symbols of a desired and of an interfering signal using the same SF do not completely overlap. Due to these characteristics of intra-SF interference, the latter is approximated by the interference created only from the dominant intra-SF interferer, in the present paper. Moreover, the inter-SF interference is neglected. Both assumptions are typical in the literature [4], [6], [8], while the accuracy of the dominant interferer approximation (versus that of the aggregate interference of all intra-SF and inter-SF interferers) is also verified by the Monte Carlo simulations of the present paper in Section V.

III. PERFORMANCE ANALYSIS

As already outlined, the present analysis focuses on two metrics of LoRa networks, namely, the Pcov and the ASE. The former metric quantifies the performance of the LoRa network from the transmitting ED's point of view and the latter metric from the network's point of view. Thus, the combination of both metrics can act complementarily, allowing for the holistic assessment of the network performance [5], [15], [16].

A. Coverage Probability

Considering an arbitrary ED of SF k, that is assigned to the ED by employing either of the two SF allocation schemes s, where $s \in \{\text{fa}, \text{ra}\}$, then the coverage probability is denoted by $P_{\text{cov}}(\gamma_{\text{D},k}, s)$ and refers to the probability that both the SIR and the SNR are greater than the respective reliability thresholds. Hence, the P_{cov} is formally formulated as [20]:

$$P_{\text{cov}}(\gamma_{\text{D},k}, s) = \Pr\{\text{SIR}_{k,s} \geq \gamma_{\text{I}},\ \ \text{SNR}_k \geq \gamma_{\text{D},k}\},$$

$$\text{SIR}_{k,s} = \frac{P_{\text{tx}} S_{0,k}}{P_{\text{tx}} I_{k,s}} = \frac{P_{\text{tx}} h_{0,k}^2 / L_{0,k}}{P_{\text{tx}} \max\limits_{i \in \Psi_{k,s}^{\mathcal{A}} \setminus (0)} \left\{ \frac{h_{i,k}^2}{L_{i,k}} \right\}},$$
$$\text{SNR}_k = P_{\text{tx}} S_{0,k} / \sigma^2, \tag{3}$$

where $\Pr\{.\}$ is the probability operator; $\gamma_{\text{D},k}$ is the QoS threshold and is a function of the spreading factor k [2]; γ_{I} is the interference rejection threshold and is independent of the SF due to the lack of inter-SF interference. In LoRa, the receiver can successfully decode the desired signal provided that the SIR over the intra-SF interferers is greater than 1 dB, i.e., $\gamma_{\text{I}} = 6$ dB [4], P_{tx} is the transmit power of all EDs; $S_{0,k}$ is the signal from the ED of interest to the gateway; $I_{k,s}$ is the interference from the dominant interferer among the transmitting EDs of SF k, while k is assigned under the SF allocation scheme s. $h_{0,k}^2$, $h_{i,k}^2$, $L_{0,k}$ and $L_{i,k}$ are the small-scale fading and large-scale path-loss from the ED of interest 0 and from the interfering ED i of SF k. $\Psi_{k,s}^{\mathcal{A}} \setminus (0)$ is the set of active (i.e. transmitting) EDs excluding the ED of interest 0, while $\Psi_{k,s}^{\mathcal{A}}$ follows an homogeneous PPP which density $\lambda_{k,s}^{\mathcal{A}} = \rho_k^A \lambda_k^s$, $s \in \{\text{fa}, \text{ra}\}$ in $\mathcal{Q}$. Here, $\rho_k^A = \frac{1}{T_{\text{in},k}} \frac{L_{\text{pac},k}}{\mathcal{R}_k}$ is the probability that an ED of SF k is active (i.e. in transmission mode); $T_{\text{in},k}$ is the average packet inter arrival time and it is assumed to be the same for all SFs, i.e., $T_{\text{in},k} = T_{\text{in}}, \forall k$; $\mathcal{R}_k$ is the bit rate of SF k and is given by $\mathcal{R}_k = k \frac{\text{Bw}}{2^k} \frac{4}{4+\text{Cr}}$ [2]; and $L_{\text{pac},k}$ is the packet length (in bits) of SF k and is given by [21]

$$L_{\text{pac},k} = k\left((N_{\text{pre}} + 4.25) + 8 + \max\left\{\left\lceil \frac{8PL - 4k + 28 + 16CRC - 20H}{4k} \right\rceil (4+\text{Cr}), 0\right\}\right), \tag{4}$$

where N_{pre} is the number of preamble symbols; PL is the physical payload length (in bytes); Cr $\in \{1,\ldots,4\}$ is the coding rate; CRC indicates the presence (i.e. $CRC = 1$) or absence (i.e. $CRC = 0$) of a cyclic redundancy check (CRC) field. $H = 0$, indicates that the header is enabled and $H = 1$ that it isn't. $\lceil\cdot\rceil$ and max are the ceiling and maximum functions, respectively. $\sigma^2 = 10^{(-174+\text{NF}+10\log_{10}\text{Bw})/10}$ [4] is the variance of the Additive White Gaussian Noise (AWGN); NF is the noise figure (in dBm) at the receiver, Bw is the transmission bandwidth and $\log_{10}(.)$ is the logarithm base 10 function. Table I summarizes main notations/symbols that are used throughout the paper.

The Pcov in (3), explicitly takes into account the correlation between the SIR and the SNR at the receiver, which was either not taken into account hitherto [4], [6], [8], or was introduced employing the signal-to-interference-plus-noise ratio (SINR), giving rise to intractable mathematical frameworks for the derivation of the Pcov [5].

Employing the formulation of (3), the Pcov is hereafter computed both under an exact and under an approximate framework.

1) Exact Framework: In order to compute Pcov employing (3), the distribution of both random variables, i.e. of the intended signal $S_{0,k}$ and of the interference $I_{k,s}$ needs to be derived. The following two Lemmas define the cumulative distribution function (CDF) of the interference from the dominant interferer and the CDF and probability density function (PDF) of the desired signal from the ED of interest.

Lemma 1: Let us denote by $\gamma(.,.)$ the lower incomplete gamma function, and $\delta = 2/\beta$. Then, the CDF $F_{S_{0,k}}(x)$ and the PDF $f_{S_{0,k}}(x)$ of the signal from the intended ED are given by

$$\begin{aligned} F_{S_{0,k}}(x) &= (\Gamma(m))^{-1}\left(\gamma(m,\mathcal{C}x) - \mathcal{A}x^{-\delta}\gamma(\delta+m,\mathcal{C}x)\right), \\ f_{S_{0,k}}(x) &= (\delta\mathcal{A}/\Gamma(m))\, x^{-\delta-1}\gamma(\delta+m,\mathcal{C}x), \end{aligned} \tag{5}$$

where $\mathcal{A} = \frac{1}{R^2}\left(\frac{K_0}{\theta}\right)^{-\delta}$, $\mathcal{C} = R^\beta\left(\frac{K_0}{\theta}\right)$ and $\Gamma(.)$ is the Gamma function.

Proof: See Appendix A. □

Lemma 2: Let us denote by $\mathcal{G}_{k,s} = \lambda^{\mathcal{A}}_{k,s}\pi R^2 = \rho^A_k p^s_k \lambda \pi R^2 = \rho^A_k \overline{N}_{k,s}$, $\overline{N}_{k,s}$ is the average number of active EDs of SF k under the SF allocation scheme s. The CDF of the strongest interferer is then given by

$$F_{I_{k,s}}(x) = \exp\left(-\mathcal{D}_{k,s}x^{-\delta}\frac{\gamma(\delta+m,\mathcal{C}x)}{\Gamma(m)} - \mathcal{G}_{k,s} + \mathcal{G}_{k,s}\frac{\gamma(m,\mathcal{C}x)}{\Gamma(m)}\right), \tag{6}$$

where $\mathcal{D}_{k,s} = \mathcal{A}\mathcal{G}_{k,s}$ and $\exp(.)$ is the exponential function.

Proof: See Appendix B. □

Having obtained the distribution of both random variables, the Pcov of an arbitrary ED of SF k under scheme s can then be computed by (7), as shown at the top of the next page, and $\mathcal{B}_k = \sigma^2\gamma_{\text{D},k}/P_{\text{tx}}$.

2) Approximation Framework: The expression of (7), and particularly the involved integral cannot be computed in closed-form, even for the simplest case of $m = 1$ (Rayleigh fading). Therefore, a tractable approximation is introduced which allows for the computation of the Pcov and of the ASE in closed-form. This will allow for unveiling the trends of these metrics with respect to key network parameters such as λ and P_{tx}. In order to develop this approximate framework, it is noted that in LoRa networks, the impact of the large-scale path-loss is much more dominant than the impact of the small-scale fading due to the long transmission distances. Hence, the mathematical framework derived in this section takes into account the long-term characteristic of the small-scale fading, i.e., its expectation, in place of the instantaneous value. In Section V, we show that the accuracy of the proposed approximation holds over a wide range of parameters. The approximated Pcov for an ED of SF k under scheme s, denoted by $\widetilde{P_{\text{cov}}}(\gamma_{\text{D},k}, s)$ can then be computed employing Proposition 1.

Proposition 1: Let us define as $\widetilde{S}_{0,k}(x)$ and $\widetilde{I}_{k,s}(x)$ the approximated desired signal and dominant interference among all transmitting ED of SF k, respectively. The approximated Pcov denoted by $\widetilde{P_{\text{cov}}}(\gamma_{\text{D},k}, s)$ is then given by (8), as shown at the top of the next page. Here $\widetilde{\mathcal{A}} = \frac{1}{R^2}\left(\frac{K_0}{\mathcal{F}}\right)^{-\delta}$, $\widetilde{\mathcal{C}} = \frac{\mathcal{F}}{R^\beta K_0}$, $\widetilde{\mathcal{D}}_{k,s} = \widetilde{\mathcal{A}}\mathcal{G}_{k,s}$, $\mathcal{F} = m\theta$, $\max\{.\}$ is the maximum function and $\mathbf{1}(x)$ is the indicator function which is equal to 1 if $x > 0$ and equal to 0 otherwise.

Proof: See Appendix C. □

B. Area Spectral Efficiency

The area spectral efficiency (in bit/s/m^2) quantifies the network information rate per unit area that meets the minimum QoS objectives, as imposed by the reliability thresholds $\gamma_{\text{D},k}$ and γ_{I}. Mathematically, the exact ASE of the considered networks under scheme $s \in \{\text{fa}, \text{ra}\}$ is given by [22]:

$$\begin{aligned} \text{ASE}_s &= \sum\nolimits_{k=7}^{12} \rho^A_k p^s_k \lambda \mathcal{R}_k P_{\text{cov}}(\gamma_{\text{D},k}, s) \\ &= \sum\nolimits_{k=7}^{12} \lambda^{\mathcal{A}}_{k,s}\mathcal{R}_k P_{\text{cov}}(\gamma_{\text{D},k}, s) = \sum\nolimits_{k=7}^{12} \text{ASE}_{k,s}. \end{aligned} \tag{9}$$

Similarly, by replacing the exact $P_{\text{cov}}(\gamma_{\text{D},k}, s)$ with the approximate $\widetilde{P_{\text{cov}}}(\gamma_{\text{D},k}, s)$ into (9) we obtain the approximated ASE denoted by $\widetilde{\text{ASE}}_s$. In the next section, the trends and behaviors of both the Pcov and the ASE are examined, employing the introduced approximate framework that allows for the derivation of closed form expressions. The exact framework, is also presented for comparison whenever possible.

IV. Performance Trends

The main goal of the present section is to investigate the impact of two key parameters of the network, namely, of the ED density and of the ED transmit power, on the performance of the two previously derived metrics that is the Pcov and the ASE. In this course, we delve into the behavior of Pcov and ASE by employing the approximate framework of (8). The Pcov is the same for all SFs and for both SF allocation schemes considered, hence the subscripts k and s can be skipped from Pcov for simplicity in the notation. Similarly, according to (9), the ASE is derived by summing up Pcov multiple times over different regions. Since Pcov is identical in every region then

the subscripts k and s affect only the scaling factors in the summation of these identical terms, while the ASE depends on all of these summed terms and not explicitly on a single k. Hence, k and s can also be skipped altogether from ASE for simplicity in the notation. We therefore, employ the following simplified notation $\widetilde{P_{\text{cov}}}\left(\gamma_{\text{D},k}, s\right) = \widetilde{\mathcal{P}}$ and $\widetilde{\text{ASE}}_{k,s} = \widetilde{\mathcal{S}}$.

A. Coverage Probability

The trends of the coverage probability $\widetilde{P_{\text{cov}}}\left(\gamma_{\text{D},k}, s\right)$ under the impact of the density of EDs λ and of the ED transmit power P_{tx} are examined in Propositions 2 and 3.

Proposition 2: Let us define $\omega = \lambda$, then the following hold: i) $\widetilde{\mathcal{P}}\left(\omega\right)$ is a convex monotonically decreasing function of ω; ii) $\widetilde{\mathcal{P}}\left(\omega \to +\infty\right) = 0$ and iii) $\widetilde{\mathcal{P}}\left(\omega \to 0\right) = \widetilde{\mathcal{A}}\left[\left(\max\left\{\mathcal{B}, \gamma_{\text{I}}\widetilde{\mathcal{C}}\right\}\right)^{-\delta}\right] + \left(\left(\max\left\{\widetilde{\mathcal{C}}, \mathcal{B}\right\}\right)^{-\delta} - \left(\gamma_{\text{I}}\widetilde{\mathcal{C}}\right)^{-\delta}\right)\mathbf{1}\left(\gamma_{\text{I}}\widetilde{\mathcal{C}} - \mathcal{B}\right)\Big]$.

Proof: See Appendix D. □

The exact expression of (7) can also be employed to prove the monotonically decreasing behavior of the Pcov, however, the second derivative of (7), cannot be computed, hence the convexity of the Pcov could not be proven hitherto. This highlights the impact of the approximate $\widetilde{P_{\text{cov}}}\left(\gamma_{\text{D},k}, s\right)$ and of Proposition 2 on the system level analysis.

From the asymptotic behavior of Pcov in Proposition 2, it is demonstrated that the Pcov converges to an upper bound when the system is sparsely-loaded, i.e. when $\lambda \to 0$. This bound is, in general, not equal to one due to the impairment of noise. Nevertheless, Pcov will approach one if we increase the transmit power so that $\mathcal{B} \to 0$, where $\mathcal{B}_k = \sigma^2\gamma_{\text{D},k}/P_{\text{tx}}$. Proposition 2 also evinces that network densification is simply destructive for the Pcov due to the increase of interference.

Proposition 3: Let us define $\xi = P_{\text{tx}}$, then the following hold: i) $\widetilde{\mathcal{P}}\left(\xi\right)$ is a concave monotonically increasing function of ξ; ii) $\widetilde{\mathcal{P}}\left(\xi \to +\infty\right) = \left(\mathcal{G}\right)^{-1}\left(\gamma_{\text{I}}\right)^{-\delta}\left(1 - \exp\left(-\mathcal{G}\right)\right) + \exp\left(-\mathcal{G}\right)\left(1 - \left(\gamma_{\text{I}}\right)^{-\delta}\right)$ [2] and iii) $\widetilde{\mathcal{P}}\left(\xi \to 0\right) = 0$.

Proof: See Appendix E. □

[2] The behavior of the Pcov when $P_{\text{tx}} \to \infty$ is influenced in practice by the practical limitations of the transceiver hardware. Therefore all presented insights need to be examined by considering the effect of the hardware limitations at this asymptotic case.

It is evident that the exact expression of (7) cannot be employed to study the trends and behavior of the Pcov with respect to P_{tx} due to the complexity of the function inside the integral. Examining Propositions 2 and 3 it can be seen that there exists an antipodal behavior of the Pcov under the density of EDs and under the ED transmit power. In particular, Pcov approaches its peak when the transmit power goes to infinity, whereas it reaches its peak when λ goes to zero. On a different note, the maximum value of Pcov is not equal to one in general, neither as a function of λ nor as a function of P_{tx}. A valuable conclusion drawn from the previous analysis is that, in order to maximize Pcov, the following two conditions need to be satisfied concurrently, that is, $P_{\text{tx}} \gg 1$ and $\lambda \ll 1$.

Propositions 2 and 3 study separately the influence of Ptx and of λ on Pcov. Although these findings give rise to several conclusions that are valuable for system design, the joint effect of the two parameters on Pcov, needs to be examined as well, to demonstrate whether any joint optimum exists or any common behavior over both parameters that cannot be revealed by the standalone analyses. Moreover, the joint asymptotic cases need to be examined as well, when for instance both $P_{\text{tx}} \to \infty$ and $\lambda \to \infty$. Hence, in the following Proposition, we study the trends of Pcov under the joint effect of both λ and P_{tx}.

Proposition 4: Let us define $\omega = \lambda$ and $\xi = P_{\text{tx}}$, then the joint coverage probability denoted by $\widetilde{\mathcal{P}}\left(\omega, \xi\right)$ is neither jointly convex nor jointly concave and no optimal pair (ω, ξ) exists, that maximizes Pcov.

Proof: See Appendix F. □

Proposition 4 evinces that no optimal pair (ω, ξ) exists, that maximizes Pcov. Hence, the standalone analyses of propositions 2 and 3, suffice for the separate optimization of Pcov with respect to each of the two parameters P_{tx} and λ.

B. Area Spectral Efficiency

Having concluded the Pcov analysis, the present section, investigates the impact of λ and of P_{tx} on the behavior and trends of the ASE, employing the approximate framework defined by $\widetilde{\text{ASE}}_{k,s} = \widetilde{\mathcal{S}}$. The impact of λ on the ASE is examined in Proposition 5 while the behavior of the ASE with respect to P_{tx} follows the behavior of the Pcov with respect to P_{tx}. Hence, the trends of the ASE with respect to P_{tx} can

$$P_{\text{cov}}\left(\gamma_{\text{D},k}, s\right) = \frac{\delta\mathcal{A}}{\Gamma\left(m\right)}\exp\left(-\mathcal{G}_{k,s}\right)\int_{x=\mathcal{B}_k}^{\infty} x^{-\delta-1}\gamma\left(\delta+m, \mathcal{C}x\right) \times \exp\left(\frac{\mathcal{D}_{k,s}x^{-\delta}\left(\gamma_{\text{I}}\right)^{\delta}\gamma\left(\delta+m, x\mathcal{C}\left(\gamma_{\text{I}}\right)^{-1}\right)}{\Gamma\left(m\right)} + \frac{\mathcal{G}_{k,s}\gamma\left(m, x\mathcal{C}\left(\gamma_{\text{I}}\right)^{-1}\right)}{\Gamma\left(m\right)}\right)dx. \tag{7}$$

$$\widetilde{P_{\text{cov}}}\left(\gamma_{\text{D},k}, s\right) = \Pr\left\{\frac{\widetilde{S}_{0,k}}{\widetilde{I}_{k,s}} \geq \gamma_{\text{I}}, \frac{P_{\text{tx}}\widetilde{S}_{0,k}}{\sigma^2} \geq \gamma_{\text{D},k}\right\} = \left(\mathcal{G}_{k,s}\right)^{-1}\left(\gamma_{\text{I}}\right)^{-\delta}\left(1 - \exp\left(-\left(\gamma_{\text{I}}\right)^{\delta}\widetilde{\mathcal{D}}_{k,s} \times \left(\max\left\{\mathcal{B}_k, \gamma_{\text{I}}\widetilde{\mathcal{C}}\right\}^{-\delta}\right)\right)\right) + \widetilde{\mathcal{A}}\exp(-\mathcal{G}_{k,s})\left(\left(\max\left\{\widetilde{\mathcal{C}}, \mathcal{B}_k\right\}\right)^{-\delta} - \left(\gamma_{\text{I}}\widetilde{\mathcal{C}}\right)^{-\delta}\right)\mathbf{1}\left(\gamma_{\text{I}}\widetilde{\mathcal{C}} - \mathcal{B}_k\right), \tag{8}$$

be studied employing the framework already derived for the Pcov, and are therefore stated, hereafter, without additional derivations.

Proposition 5: Let us define $\omega = \lambda$, then the following conclusions hold; i) If $\mathcal{B} < \gamma_{\rm I}\widetilde{\mathcal{C}}$, then $\widetilde{\mathcal{S}}(\omega)$ is a unimodal function, attaining its maximum at $\omega^* = \upsilon(1)$ where

$$\upsilon(x) = \left(x + (\gamma_{\rm I})^{-\delta}\left[\widetilde{\mathcal{A}}\left(\left(\max\left\{\widetilde{\mathcal{C}}, \mathcal{B}\right\}\right)^{-\delta} - \left(\gamma_{\rm I}\widetilde{\mathcal{C}}\right)^{-\delta}\right)\right]^{-1}\right) \times \left(\rho^{\mathcal{A}}\pi R^2\right)^{-1}.$$

Additionally, the ASE changes from a concave function of ω into a convex function at the inflection point $\omega^{**} = \upsilon(2)$; ii) If $\mathcal{B} \geq \gamma_{\rm I}\widetilde{\mathcal{C}}$, then the ASE is a concave increasing function of ω; iii) In the asymptotic case of the interference-limited regime, namely when $\omega \to \infty$ the ASE is given by $\widetilde{\mathcal{S}}(\omega \to +\infty) = (\gamma_{\rm I})^{-\delta}\mathcal{R}/\left(\pi R^2\right)$ and iv) The ASE does not go to zero unless the ED density goes to zero, i.e. $\widetilde{\mathcal{S}}(\omega \to 0) = 0$.

Proof: See Appendix G. □

Proposition 5 demonstrates that the mathematical framework for deriving both critical points, i.e., ω^* and ω^{**}, is identical. Additionally, since $\omega^* < \omega^{**}$, this means that the maximum ω^* resides in the concave region of the function. Examining Propositions 2 and 5, it becomes evident that with respect to λ, ASE and Pcov exhibit a very different behaviour. Specifically, ASE is either a monotonically increasing or a unimodal function of λ, while Pcov is simply a decreasing function of λ. Proposition 5 demonstrates that when the ASE is a unimodal function of λ, the optimum λ, maximizing the ASE can be computed in closed-form. Building upon that finding, we hereafter examine how the value of the path-loss exponent β affects this optimal value of λ. In this direction, the following Corollary is stated.

Corollary 1: Examining $\upsilon(x)$ defined in Proposition 5, it is evinced that $\upsilon(x)$ increases with β if $\mathcal{F} \geq K_0 \exp\left(-\frac{\ln(\gamma_{\rm I}/z)}{1-(\gamma_{\rm I}/z)^{-1}}\right)$, where $z = \mathcal{B}$ for $\widetilde{\mathcal{C}} \leq \mathcal{B} \leq \gamma_{\rm I}\widetilde{\mathcal{C}}$ and $z = 1$ for $\widetilde{\mathcal{C}} > \mathcal{B}$.

Proof: See Appendix H. □

Having concluded the analysis of the standalone impact of λ on the ASE, the following two propositions examine the trends of the ASE as a standalone function of $P_{\rm tx}$ and as a joint function of λ and $P_{\rm tx}$.

Proposition 6: Let us define $\xi = P_{\rm tx}$, then $\widetilde{\mathcal{S}}(\xi)$ is a concave monotonically increasing function of ξ. Additionally, $\widetilde{\mathcal{S}}(\xi)$ approaches its upper bound

$$\lambda^{\mathcal{A}}\mathcal{R}\left((\mathcal{G})^{-1}(\gamma_{\rm I})^{-\delta}(1-\exp(-\mathcal{G})) + \exp(-\mathcal{G})\left(1-(\gamma_{\rm I})^{-\delta}\right)\right)$$

when $\xi \to +\infty$ and its lower bound 0 when $\xi \to 0$.

Propositions 3 and 6 demonstrate the similarity between the behaviors of the ASE and Pcov functions with respect to $P_{\rm tx}$. However, Propositions 2 and 5 demonstrated that the two curves have a different behaviour with respect to the density of EDs. Hence, it is natural to raise the question, whether the behavior of ASE with respect to both λ and $P_{\rm tx}$ is also analogous to that of Pcov or not. That is, whether it is also universally neither jointly convex nor jointly concave. The answer is provided by the following proposition.

Proposition 7: Let us define $\omega = \lambda$ and $\xi = P_{\rm tx}$, then the following statements are true: i) the ASE is not characterized by a common universal behavior over the whole domain. Hence, there are regions where the ASE is neither jointly convex nor jointly concave and other regions where the same behaviour is exhibited with respect to both parameters ω and ξ. ii) In the region where the ASE is jointly concave a set of joint optimums exist maximizing the ASE over both ω and ξ. This set of joint optimums is defined by the segment $\xi^* \geq \frac{\sigma^2\gamma_{\rm D}}{\mathcal{C}}$ and $\omega^* = \left(\rho^{\mathcal{A}}\pi R^2\right)^{-1}(1+\phi_1/\phi_3)$, in which the ASE attains its maximum value, where $\phi_1 = (\gamma_{\rm I})^{-\delta}$ and $\phi_3 = \widetilde{\mathcal{A}}\left(\left(\max\left\{\widetilde{\mathcal{C}}, \mathcal{B}\right\}\right)^{-\delta} - \left(\gamma_{\rm I}\widetilde{\mathcal{C}}\right)^{-\delta}\right)$.

Proof: See Appendix I. □

V. Numerical Results

The present section provides the numerical results corroborating the validity of the considered assumptions while substantiating the findings of Section IV demonstrating the accuracy of the derived mathematical framework. In this course, a LoRa network of IoT devices is simulated, that is a home security system, that is characterized by the transmission parameters that are explicitly defined by the in-home machine to machine (M2M) communications framework. In particular, in the present section (unless otherwise stated) the following setup is considered [24]: $\beta = 2.9$, Bw = 125 kHz, NF = 6 dBm, $\gamma_{\rm I} = 6$ dB, $f_c = 868$ MHz, $R = 2000$ m, $m = 3.5$[3], $\Omega = 9.5$, $\overline{N} = 4000$, $P_{\rm tx} = 10$ dBm, $PL = 20$ bytes, $N_{\rm pre} = 8$, $CRC = 1$, $H = 0$, Cr = 1 and $T_{\rm in} = 600$ seconds.

Figure 1 depicts the Pcov and the ASE as a function of the transmit power under the random SF allocation scheme and under various small-scale fading distributions, i.e., Rayleigh fading ($m = 1$, $\theta = 2.7144$) and no fading ($m = 15$, $\theta = 2.7144$). The accuracy of the proposed mathematical frameworks is verified by Monte Carlo simulations. Evidently, the approximate frameworks defined by equation (8) and the ensuing approximate expression for the ASE, give rise to curves that are very close to those of the exact frameworks arising from (7) and (9). Moreover, if the SINR-based approach would be adopted, it would coincide with the "Sum" curves and would serve as a lower bound of the proposed approximate framework [20]. We also observe that the approximation of the interference by the dominant interferer, that is employed in the approximate framework, is tight since it exactly coincides with the exact framework that employs the aggregate interference particularly in the no fading case (where the fading approximation does not affect the results). Moreover, as expected, when fading is present, the system performs worse that in the case of no fading, while the performance of both systems converges when $P_{\rm tx}$ increases substantially. That is, since for a high $P_{\rm tx}$ the SNR surpasses the respective threshold regardless of the presence or absence

[3]Recently, the authors of [25] proved that even in harsh propagating environments, i.e., indoor environments, the multi-path propagation in LoRa systems is still dominated by a single component of the signal and that the Rayleigh distribution is not an appropriate distribution for modelling the fast fading in LoRa networks. Consequently, the fading severity $m = 3.5$ is selected in the present paper.

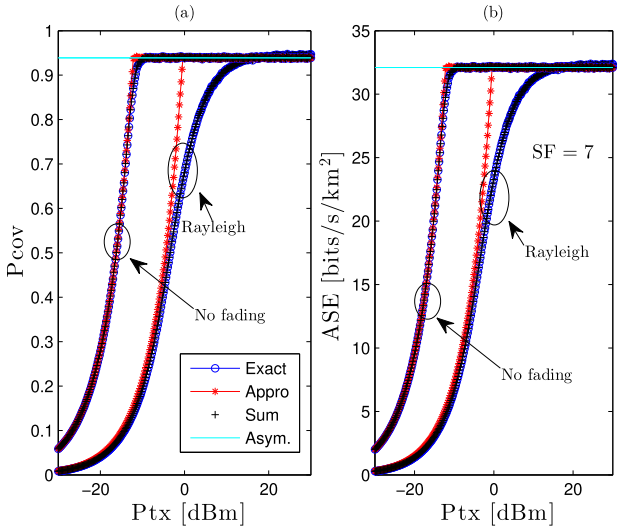

Fig. 1. Coverage probability (a) and area spectral efficiency (b) versus the transmit power under random SF allocation scheme. The marked solid lines show the exact, and approximate analytical framework, while the plain solid line shows the asymptotic behavior when $P_{\text{tx}} \to \infty$ for both the Pcov and ASE as computed by equations (7), (8) and (9). The markers show the respective Monte Carlo simulations.

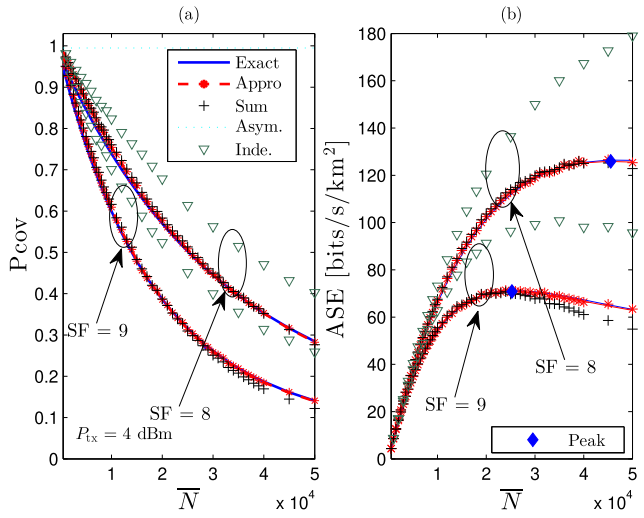

Fig. 2. Coverage probability (a) and area spectral efficiency (b), versus the average number of ED $\overline{N}$ under random SF allocation scheme. The solid lines correspond to the exact framework computed by (7), (9); the dashed lines correspond to the approximate framework computed by (8) and (9) and the downward-pointing triangles correspond to the popular approximation that ignores the correlation between the SNR and the SIR at the receiver (that is computed by Monte Carlo simulations). The plus sign markers show the Monte Carlo simulations accounting for the aggregate interference intra-SF interference. The dotted lines show the asymptotic behavior defined in Proposition 2 as $\overline{N} \to 0$. The diamond markers indicate the maximum ASE defined in proposition 5.

of fading. In that case, the performance of Pcov and ASE is independent of the small-scale fading distributions. The figure also confirms the finding of Propositions 3 and 6 that both the Pcov and ASE converge to a maximum value as P_{tx} tends to infinity.

Figure 2 illustrates the performances of Pcov and ASE with respect to the average number of EDs $\overline{N}$ (which in turn defines λ) under random SF allocation and for different SF indices. Again, there is a tight matching between the mathematical framework and the computer-based simulations, with the introduced approximation of the Pcov practically coinciding with the exact curve, as opposed to the popular approximation of [4], [6], [8] that ignores the correlation between the SNR and the SIR at receiver (denoted by "Inde") that deviates significantly from the exact curve as the ED density increases. The "Sum", again, serves as the lower bound of these curves and will coincide with the SINR-based definition (if considered). Fig. 2(a) verifies the finding of Proposition 2 that Pcov decreases as $\overline{N}$ increases. Thus, demonstrating that network densification has a detrimental effect to the coverage probability. Additionally, under random SF allocation scheme it can be seen that as the SF increases the Pcov and the ASE decrease. The reason is that the packets of larger SFs are being transmitted for a longer period of time, thus experiencing more interference. Also figure 2 depicts the asymptotic behaviour of the Pcov when $\overline{N}$ goes to zero. Figure 2(b) illustrates the performance of the ASE versus $\overline{N}$, for different SFs. As expected, the ASE of the lower SF significantly outperforms the ASE of the higher SF, due to the corresponding performance gap of the two respective Pcov. Moreover, this figure also corroborates the finding of Proposition 5 that the ASE is either a unimodal or an increasing function of $\overline{N}$ (or λ). The optimal value of $\overline{N}$, denoted by $\overline{N}^*$ which is computed in Proposition 5 is also plotted in Figure 2(b) (with the marker "♦"). The optimal value of $\overline{N}$ demonstrates that the value of $\overline{N}$ that maximizes the ASE is a value where the Pcov of a standalone ED significantly decreases due to the number of surrounding EDs. This antipodal behavior demonstrates that since LoRa networks do not include a single ED but a multitude of them, the ASE is a more sensible figure of merit for network design. Thus, implicitly highlighting the importance of Proposition 7, for network design, that derives in closed form the joint global optimum that maximizes the network ASE.

As opposed to Figure 2, Figure 3(a) demonstrates that, under a fair-collision scheme, the Pcov of a smaller SF is not constantly superior to that of a larger SF. Particularly, before the asymptotic regime the Pcov of a higher SF is higher than the Pcov of a lower SF. The reason for that is that the respective reliability threshold is higher for a lower SF, i.e., $\gamma_{\text{D},7} > \gamma_{\text{D},12}$, whereas the transmit power and the background noise are the same. Hence, (if not at the asymptotic regime) the SNR of the lower SF is more difficult to exceed the higher reliability threshold. However, at the asymptotic regime, when Ptx is high enough for the SNR to always exceed the reliability threshold, the impact of the SIR comes into play, and the Pcov of the lower SF outperforms its counterpart of high SF by virtue of the higher activation probability ρ_k^A in the latter case that entails an increased interference by active intra-SF EDs. This figure also reveals that the adopted approach accounting only for the dominant intra-SF interferer serves as a tight upper bound of the approach accounting for the aggregate interference of all inter-SF and intra-SF interferers. Fig. 3(b) depicts the summed ASE (that arises by the summation over all SFs) versus the ED transmit power P_{tx}. As evinced by

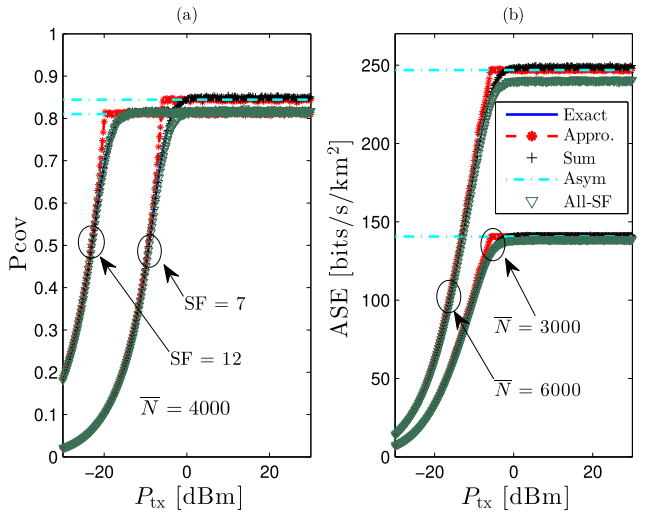

Fig. 3. Coverage probability (a) and area spectral efficiency (b), versus P_{tx} under a fair-collision SF allocation scheme. The solid lines correspond to the exact framework of (7), and (9); the dashed lines show the approximate framework of (8) and (9) and the dotted dashed lines show the asymptotic behavior as $P_{\text{tx}} \rightarrow \infty$. The plus sign markers show the Monte Carlo simulations accounting only for the aggregate interference intra-SF interferer, while the downward-pointing triangles show the simulations considering the aggregate interference (of all inter-SF and intra-SF interferers).

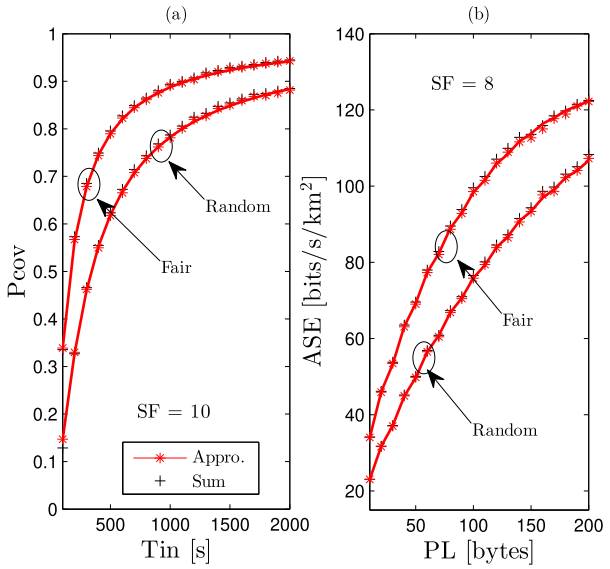

Fig. 4. Coverage probability versus T_{in} (a) and area spectral efficiency versus PL (b), under both random and fair SF allocation schemes. Solid lines show approximation framework (8), (9). Markers show Monte Carlo simulations.

Proposition 6 the trends of the ASE function with respect to P_{tx} are the same as the trends of the Pcov.

Figure 4 depicts the Pcov versus T_{in} and the ASE versus the PL employing the closed form expressions of (8), (9), and demonstrating a monotonic increase of both the Pcov and ASE with respect to these two parameters. More precisely, the ASE experiences a three-to-five-fold increase as the packet length increases from 10 to 200 bytes while the Pcov experiences a three-to-five-fold increase as the inter-arrival time between two packets T_{in} rises from 100 to 2000 seconds. That is since by increasing T_{in} we decrease the activation probability

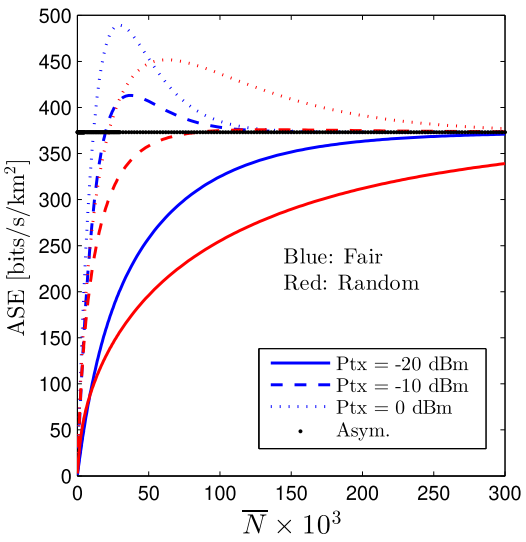

Fig. 5. The summed ASE versus $\overline{N}$ with various values of P_{tx}. Lines are plotted by approximation framework (8), (9). Marker shows the asymptotic framework in proposition 5.

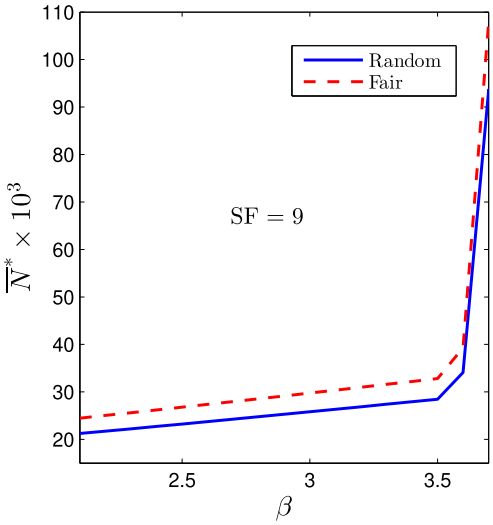

Fig. 6. $\overline{N}^*$ versus β with SF $= 9$ and $P_{\text{tx}} = 10$ dBm. Curves are plotted base on $\upsilon\,(1)$ in proposition 5.

ρ_k^A, which in turn reduces the interference. Thus improving the two metrics, while intuitively quantifying the impact of the interference on both metrics. Additionally, the curves employing a fair SF allocation scheme always outperform the random SF allocation schemes for all SFs.

Figure 5 illustrates the summed ASE as a function of the average number of EDs for different values of P_{tx}. The figure confirms that the ASE is either a unimodal or a monotonically increasing function of P_{tx} as proved in Proposition 5. Moreover, the ASE always exhibits the same asymptotic behavior as $\overline{N}$ increases, regardless of the transmit power. This figure also corroborates that the fair-collision SF allocation scheme always outperforms the random SF allocation scheme.

Fig. 6 depicts the trend of the optimal value of the average number of EDs $\overline{N}^*$ corresponding to the path-loss exponent. We observe that $\overline{N}^*$ turns up when β goes up and confirms

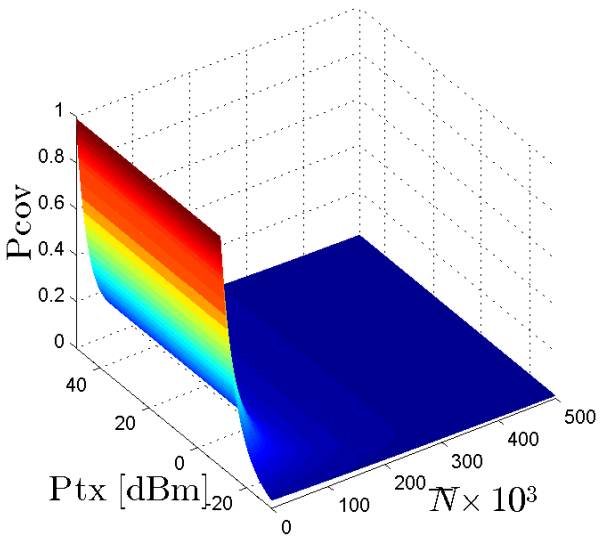

Fig. 7. The coverage probability as a function of both the average number of EDs $\overline{N}$ and the transmit power P_{tx} under fair SF allocation scheme for SF$k = 8$.

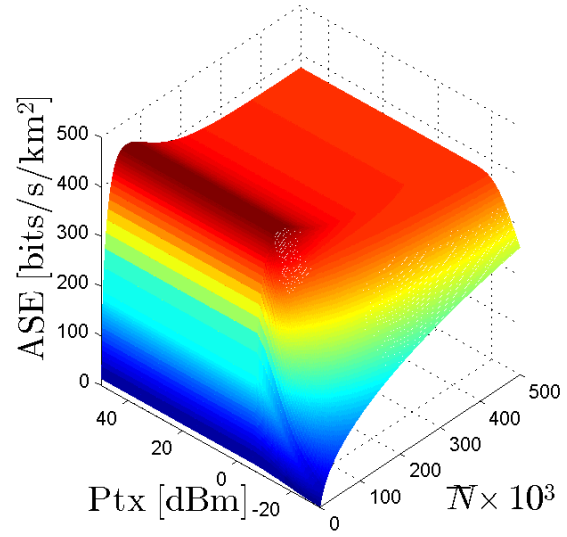

Fig. 8. The summed area spectral efficiency as a function of both the average number of EDs $\overline{N}$ and the transmit power P_{tx} under random SF allocation scheme.

our findings in Corollary 5. Additionally, the fair-collision is better than its counterpart due to $p_9^{\text{fa}} < p_9^{\text{ra}}$.

Figure 7 shows the Pcov under a fair SF allocation scheme for SF $k = 8$. The figure corroborates the findings of Proposition 4, since the joint coverage probability is indeed neither jointly convex nor jointly concave and no optimal pair (ω, ξ) exists, that maximizes Pcov, apart from the asymptotic case of $\overline{N} \to 0$.

Figure 8 shows the summed ASE under a random SF allocation scheme with respect to both $\overline{N}$ and P_{tx}. As already evinced in Proposition 7 the ASE is not characterized by any common universal behavior over the whole domain, with regions where the ASE is neither jointly convex nor joinlty concave and other regions where the same behaviour is exhibited with respect to both parameters. More importantly as already evinced, in the region where the ASE is jointly concave a set of joint optimums exist maximizing the ASE over both $\overline{N}$ and P_{tx} and this set of joint optimums is the one defined in Proposition 7, where the ASE attains its maximum value.

VI. Conclusion

The derived, closed-form framework, fully characterizes the system Pcov and ASE, with respect to the transmit power P_{tx} and the ED density λ under different SF allocation schemes, and even in the asymptotic cases. More importantly it evinces that no joint optimum exists that maximizes the Pcov with respect to both parameters, but that the standalone optimization of the two parameters needs to be followed. As opposed to that it is proven that a joint optimum exists that maximizes the ASE, which constitutes a figure of merit that quantifies the overall network performance. This joint optimum is defined in closed form. Thus the derived framework arises as an important tool, of significant practical value, for the optimization of the network deployment and for the transceiver design in IoT LoRa networks.

Appendix A
Proof of Eq. (5)

In this section, the CDF and PDF of $S_{0,k}$ are derived. Let us start with the definition of the CDF as follows:

$$\begin{aligned} F_{S_{0,k}}(x) &= \Pr\left\{h_{0,k}^2 / \left(K_0 r_{0,k}^{\beta}\right) < x\right\} \\ &= \Pr\left(h_{0,k}^2 < x K_0 r_{0,k}^{\beta}\right) \\ &\overset{(a)}{=} \frac{1}{\Gamma(m)} \frac{2}{R^2} \frac{1}{\beta} \int_{t=0}^{R^{\beta}} \gamma\left(m, \frac{xK_0 t}{\theta}\right) t^{\delta-1} dt \\ &\overset{(b)}{=} \gamma(m, \mathcal{C}x)/\Gamma(m) - \mathcal{A}x^{-\delta}\gamma(\delta+m, \mathcal{C}x)/\Gamma(m), \end{aligned} \tag{10}$$

where (a) is obtained by employing the CDF of the small-scale fading $h_{0,k}^2$ and the PDF of the distance $r_{0,k}$ from the intended ED to the gateway after changing the variable of the PDF into $t = r_{0,k}^{\beta}$; (b) arises from [27]; $\mathcal{A}, \mathcal{C}$ and δ are defined in Lemma 1. Taking the first-order derivative of $F_{S_{0,k}}(x)$ with respect to x we obtain the PDF. QED.

Appendix B
Proof of Eq. (6)

According to order statistics, assuming $i \in \mathbb{N}$ independent and identical distributed (i.i.d.) random variables with CDF $F_I(x)$, then the CDF of the maximum random variable among the i variables is given by $F_{I_{\text{M}}}(x) = (F_I(x))^i$. Moreover, the

number of active interferers of SF k under the SF allocation scheme $s \in \{\text{fa}, \text{ra}\}$ follows a Poisson distribution with mean $\mathcal{G}_{k,s} = \lambda^{\mathcal{A}}_{k,s}\pi R^2 = \rho^A_k p^s_k \lambda \pi R^2 = \rho^A_k \overline{N}_{k,s}$. Hence, the CDF of the interference from the dominant interferer is given by

$$\begin{aligned} &F_{I_{k,s}}(x) \\ &\overset{(a)}{=} \exp\left(-\mathcal{G}_{k,s}\right) \sum_{i=0}^{\infty} \left[\frac{\gamma\left(m, \mathcal{C}x\right)}{\Gamma\left(m\right)} - \frac{\mathcal{A}\,\gamma\left(\delta+m, \mathcal{C}x\right)}{x^{\delta}\quad \Gamma\left(m\right)}\right]^i \frac{\left(\mathcal{G}_{k,s}\right)^i}{i!} \\ &\overset{(b)}{=} \exp\left(-\mathcal{D}_{k,s}x^{-\delta}\frac{\gamma\left(\delta+m, \mathcal{C}x\right)}{\Gamma\left(m\right)} - \mathcal{G}_{k,s} + \mathcal{G}_{k,s}\frac{\gamma\left(m, \mathcal{C}x\right)}{\Gamma\left(m\right)}\right), \end{aligned} \tag{11}$$

where (a) is attained by averaging the CDF of the maximum interference among i interferers, over all possible numbers of active interferers i; (b) employs the definition of the exponential function $\sum_{i=0}^{\infty} \frac{x^i}{i!} = \exp(x)$ [26, Eq. 1.211.1] and $\mathcal{D}_{k,s} = \mathcal{A}\mathcal{G}_{k,s}$. QED.

Appendix C
Proof of Eq. (8)

Let us commence this appendix by computing the CDF and the PDF of the approximated desired signal denoted by $\widetilde{S}_{0,k} = \mathcal{F}/L_{0,k}$ and the CDF of the interference from the dominant interferer among all transmitting EDs of SF k denoted by $\widetilde{I}_{k,s} = \max_{i \in \Psi^{\mathcal{A}}_{k,s} \setminus (0)} \{\mathcal{F}/L_{i,k}\}$. The respective CDFs and PDF are given by

$$\begin{aligned} F_{\widetilde{S}_{0,k}}(x) &= \Pr\left\{\frac{\mathcal{F}}{K_0 r^{\beta}_{0,k}} \le x\right\} \\ &\overset{(a)}{=} \left(\frac{2}{R^2}\int_{r=(\mathcal{F})^{\frac{1}{\beta}}(K_0 x)^{-\frac{1}{\beta}}}^{R} r dr\right) \\ &\quad \times \mathbf{1}\left(x - \widetilde{\mathcal{C}}\right) = \left(1 - \widetilde{\mathcal{A}}x^{-\delta}\right)\mathbf{1}\left(x - \widetilde{\mathcal{C}}\right), \\ f_{\widetilde{S}_{0,k}}(x) &= dF_{\widetilde{S}_{0,k}}(x)/dx = \delta\widetilde{\mathcal{A}}x^{-\delta-1}\mathbf{1}\left(x - \widetilde{\mathcal{C}}\right) \\ F_{\widetilde{I}_k}(x) &= \exp\left(-\mathcal{G}_{k,s}\right)\sum_{i=0}^{\infty}\left[\left(1 - \widetilde{\mathcal{A}}x^{-\delta}\right)\mathbf{1}\left(x - \widetilde{\mathcal{C}}\right)\right]^i \\ &\quad \times \frac{\left(\mathcal{G}_{k,s}\right)^i}{i!} \\ &= \exp\left(-\mathcal{G}_{k,s}\mathbf{1}\left(\widetilde{\mathcal{C}} - x\right)\right) \\ &\quad \times \times \exp\left(-\widetilde{\mathcal{D}}_{k,s}x^{-\delta}\mathbf{1}\left(x - \widetilde{\mathcal{C}}\right)\right). \end{aligned} \tag{12}$$

In (12), (a) is obtained by applying the PDF of the distance and $F_{\widetilde{I}_{k,s}}(x)$ is derived by employing the same steps as in (11).

Employing (12) the approximated coverage probability of an ED of SF k under the SF allocation scheme s is given by

$$\begin{aligned} &\widetilde{P_{\text{cov}}}(\gamma_{\text{D},k}, s) \\ &= \Pr\left\{\widetilde{S}_{0,k}/\widetilde{I}_{k,s} \ge \gamma_{\text{I}}, P_{\text{tx}}\widetilde{S}_{0,k}/\sigma^2 \ge \gamma_{\text{D},k}\right\} \\ &= \int_{x=\mathcal{B}_k}^{\infty} \delta\widetilde{\mathcal{A}}x^{-\delta-1}\exp\left(-\mathcal{G}_{k,s}\mathbf{1}\left(\gamma_{\text{I}}\widetilde{\mathcal{C}} - x\right)\right)\mathbf{1}\left(x - \widetilde{\mathcal{C}}\right) \\ &\quad \times \exp\left(-x^{-\delta}\widetilde{\mathcal{D}}_{k,s}(\gamma_{\text{I}})^{\delta}\mathbf{1}\left(x - \gamma_{\text{I}}\widetilde{\mathcal{C}}\right)\right)dx \\ &\overset{(a)}{=} J_1\left(\max\left\{\mathcal{B}_k, \gamma_{\text{I}}\widetilde{\mathcal{C}}\right\}\right) + J_2\left(\max\left\{\mathcal{B}_k, \widetilde{\mathcal{C}}\right\}, \gamma_{\text{I}}\widetilde{\mathcal{C}}\right) \\ &\quad \times \mathbf{1}\left(\gamma_{\text{I}}\widetilde{\mathcal{C}} - \mathcal{B}_k\right). \end{aligned} \tag{13}$$

Here (a) is obtained by splitting the integration into three cases, namely: i) $\gamma_{\text{I}}\widetilde{\mathcal{C}} \le \mathcal{B}_k$; ii) $\widetilde{\mathcal{C}} \le \mathcal{B}_k < \gamma_{\text{I}}\widetilde{\mathcal{C}}$ and iii) $\mathcal{B}_k < \widetilde{\mathcal{C}}$; Moreover, $J_1(a)$ and $J_2(a,b)$ are given by:

$$\begin{aligned} J_1(a) &= \int_{x=a}^{\infty} \delta\widetilde{\mathcal{A}}x^{-\delta-1}\exp\left(-x^{-\delta}\widetilde{\mathcal{D}}_{k,s}(\gamma_{\text{I}})^{\delta}\right)dx \\ &= \left(\mathcal{G}_{k,s}\right)^{-1}(\gamma_{\text{I}})^{-\delta}\left(1 - \exp\left(-(\gamma_{\text{I}})^{\delta}(a)^{-\delta}\widetilde{\mathcal{D}}_{k,s}\right)\right) \end{aligned}$$

and

$$\begin{aligned} J_2(a,b) &= \exp\left(-\mathcal{G}_{k,s}\right)\int_{x=a}^{b}\delta\widetilde{\mathcal{A}}x^{-\delta-1}dx \\ &= \widetilde{\mathcal{A}}\exp\left(-\mathcal{G}_{k,s}\right)\left((a)^{-\delta} - (b)^{-\delta}\right). \end{aligned}$$

The employment of (13) by inputting $J_1(a)$ and $J_2(a,b)$ gives (8). QED.

Appendix D
Proof of Proposition 2

Let us rewrite Pcov as a function of the ED density ω

$$\begin{aligned} \widetilde{\mathcal{P}}(\omega) &= \phi_1(\mathcal{G}(\omega))^{-1}\left(1 - \exp\left(-\phi_2\mathcal{G}(\omega)\right)\right) \\ &\quad + \phi_3\exp\left(-\mathcal{G}(\omega)\right)\mathbf{1}\left(\gamma_{\text{I}}\widetilde{\mathcal{C}} - \mathcal{B}\right). \end{aligned} \tag{14}$$

In (14), the $\widetilde{P_{\text{cov}}}(\gamma_{\text{D},k}, s)$ depends on $\omega = \lambda$, via the term $\mathcal{G}(\omega)$, which is given by $\mathcal{G}(\omega) = \rho^A\pi R^2\omega$, while the following terms of (14) are defined hereafter, and do not depend on ω: $\phi_1 = (\gamma_{\text{I}})^{-\delta}$, $\phi_2 = (\gamma_{\text{I}})^{\delta}\left(\max\left\{\mathcal{B}, \gamma_{\text{I}}\widetilde{\mathcal{C}}\right\}\right)^{-\delta}\widetilde{\mathcal{A}}$ and $\phi_3 = \widetilde{\mathcal{A}}\left(\left(\max\left\{\widetilde{\mathcal{C}}, \mathcal{B}\right\}\right)^{-\delta} - \left(\gamma_{\text{I}}\widetilde{\mathcal{C}}\right)^{-\delta}\right)$. By computing the first-order derivative of (14) with respect to ω we obtain

$$\begin{aligned} &\dot{\widetilde{\mathcal{P}}}(\omega) \\ &= -\phi_1\dot{\mathcal{G}}(\omega)\left(\mathcal{G}(\omega)\right)^{-2}[1 - \exp\left(-\phi_2\mathcal{G}(\omega)\right)(1 + \phi_2 \\ &\quad \times \mathcal{G}(\omega))] - \phi_3\dot{\mathcal{G}}(\omega)\exp\left(-\mathcal{G}(\omega)\right)\mathbf{1}\left(\gamma_{\text{I}}\widetilde{\mathcal{C}} - \mathcal{B}\right) \le 0, \quad \forall\omega \ge 0, \end{aligned} \tag{15}$$

where $\dot{f}(x) = df(x)/dx$ is the first-order derivative of f with respect to x; $\dot{\widetilde{\mathcal{P}}}(\omega) \le 0$ because, for the first-order derivative of $\mathcal{G}(\omega)$ it holds that, $\dot{\mathcal{G}}(\omega) = \rho^A\pi R^2 \ge 0$. Hence, $\widetilde{P_{\text{cov}}}(\gamma_{\text{D},k}, s)$ decreases monotonically with $\omega = \lambda$.

In order to evince the convexity of the function, we derive the second-order derivative of $\widetilde{P_{\text{cov}}}(\gamma_{\text{D},k}, s)$ denoted by $\ddot{\widetilde{\mathcal{P}}}(\omega)$, which is given by

$$\begin{aligned} \ddot{\widetilde{\mathcal{P}}}(\omega) &= \phi_3\left[\dot{\mathcal{G}}(\omega)\right]^2\exp\left(-\mathcal{G}(\omega)\right)\mathbf{1}\left(\gamma_{\text{I}}\widetilde{\mathcal{C}} - \mathcal{B}\right) + \phi_1\left[\dot{\mathcal{G}}(\omega)\right]^2 \\ &\quad \times \left(\mathcal{G}(\omega)\right)^{-3}\left(2 - \exp\left(-\phi_2\mathcal{G}(\omega)\right)\right. \\ &\quad \times \left.\left(1 + \left(1 + \phi_2\mathcal{G}(\omega)\right)^2\right)\right) \ge 0. \end{aligned} \tag{16}$$

The term $[2 - \exp\left(-\phi_2\mathcal{G}(\omega)\right)\left(1 + \left(1 + \phi_2\mathcal{G}(\omega)\right)^2\right)]$ of (16) is a monotonically increasing function of $\phi_2\mathcal{G}(\omega)$, with a

minimum that is equal to 0 (for $\phi_2\mathcal{G}(\omega)=0$). The equality in (16) holds only for $\omega\to\infty$, where

$$\begin{aligned}\ddot{\widetilde{\mathcal{P}}}(\omega\to\infty) &= \phi_3\left[\dot{\mathcal{G}}(\omega)\right]^2\underbrace{\exp\left(-\mathcal{G}(\omega)\right)}_{=0}\mathbf{1}\left(\gamma_{\mathrm{I}}\widetilde{\mathcal{C}}-\mathcal{B}\right)+\phi_1\left[\dot{\mathcal{G}}(\omega)\right]^2\\ &\quad\times\underbrace{\left(\mathcal{G}(\omega)\right)^{-3}}_{=0}\\ &\quad\times\left(2-\underbrace{\exp\left(-\phi_2\mathcal{G}(\omega)\right)\left(1+(1+\phi_2\mathcal{G}(\omega))^2\right)}_{\mathcal{V}_{10}}\right)=0\end{aligned}$$

$$\begin{aligned}\mathcal{V}_{10} &= \lim_{\omega\to\infty}\left(\frac{2+2\phi_2\mathcal{G}(\omega)+(\phi_2\mathcal{G}(\omega))^2}{\exp\left(\mathcal{G}(\omega)\right)}\right)\\ &\overset{(a)}{=} 2\phi_2\lim_{\omega\to\infty}\left(\frac{\phi_2\dot{\mathcal{G}}(\omega)}{\dot{\mathcal{G}}(\omega)\exp\left(\mathcal{G}(\omega)\right)}\right)=0,\end{aligned}\tag{17}$$

where (a) is obtained by using L'Hôpital's rule. Hence, $\widetilde{\mathcal{P}}(\omega)$ is a convex function, while $\dot{\widetilde{\mathcal{P}}}(\omega)$ is a monotonically increasing function and attains its maximum at

$$\begin{aligned}&\dot{\widetilde{\mathcal{P}}}(\omega\to\infty)\\ &= -\phi_1\left(\dot{\mathcal{G}}(\omega)\right)\frac{1-\exp\left(-\phi_2\mathcal{G}(\omega)\right)\left(1+\phi_2\mathcal{G}(\omega)\right)}{\left(\mathcal{G}(\omega)\right)^2}\\ &\quad-\phi_3\left(\mathcal{G}(\omega)\right)\exp\left(-\mathcal{G}(\omega)\right)\mathbf{1}\left(\gamma_{\mathrm{I}}\widetilde{C}-\mathcal{B}\right)=-\phi_1\left(\dot{\mathcal{G}}(\omega)\right)\\ &\quad\times\left[\underbrace{\frac{1}{\left(\mathcal{G}(\omega)\right)^2}}_{=0}-\underbrace{\frac{\exp\left(-\phi_2\mathcal{G}(\omega)\right)}{\left(\mathcal{G}(\omega)\right)^2}}_{=0}-\underbrace{\frac{\phi_2\exp\left(-\phi_2\mathcal{G}(\omega)\right)}{\left(\mathcal{G}(\omega)\right)}}_{=0}\right]\\ &\quad-\phi_3\left(\mathcal{G}(\omega)\right)\underbrace{\exp\left(-\mathcal{G}(\omega)\right)}_{=0}\mathbf{1}\left(\gamma_{\mathrm{I}}\widetilde{C}-\mathcal{B}\right)=0\end{aligned}\tag{18}$$

Since $\dot{\widetilde{\mathcal{P}}}(\omega)$ is a monotonically increasing function, from (15) and (18), we conclude that $\dot{\widetilde{\mathcal{P}}}(\omega)$ is strictly negative and becomes equal to 0 only for $\omega\to\infty$. Hence, $\widetilde{\mathcal{P}}(\omega)$ is a convex monotonically decreasing function of ω. Finally, the asymptotic behavior of Pcov when $\omega\to 0$ is given by

$$\begin{aligned}\lim_{\omega\to 0}\widetilde{\mathcal{P}}(\omega) &= \lim_{\omega\to 0}\left(\phi_1\left(1-\exp\left(-\phi_2\mathcal{G}(\omega)\right)\right)/\mathcal{G}(\omega)\right.\\ &\quad\left.+\phi_3\exp\left(-\mathcal{G}(\omega)\right)\mathbf{1}\left(\gamma_{\mathbf{I}}\widetilde{\mathcal{C}}-\mathcal{B}\right)\right)\\ &\overset{(a)}{=}\phi_1\phi_2+\phi_3\mathbf{1}\left(\gamma_{\mathbf{I}}\widetilde{\mathcal{C}}-\mathcal{B}\right),\end{aligned}\tag{19}$$

where (a) is obtained by employing L'Hôpital's rule. QED.

Appendix E
Proof of Proposition 3

At first, the approximate expression for Pcov is defined as a function of the transmit power $\xi=P_{\mathrm{tx}}$

$$\begin{aligned}\widetilde{\mathcal{P}}(\xi) &= \phi_4\left(1-\exp\left(-\phi_5(\max\left\{\mathcal{B}(\xi),\phi_7\right\})^{-\delta}\right)\right)\\ &\quad+\phi_6\left(\left(\max\left\{\mathcal{B}(\xi),\widetilde{\mathcal{C}}\right\}\right)^{-\delta}-\left(\phi_7\right)^{-\delta}\right)\\ &\quad\times\mathbf{1}\left(\phi_7-\mathcal{B}(\xi)\right),\end{aligned}\tag{20}$$

where the terms $\phi_4=(\mathcal{G})^{-1}(\gamma_{\mathrm{I}})^{-\delta},\phi_5=(\gamma_{\mathrm{I}})^{\delta}\widetilde{\mathcal{A}}\mathcal{G},\phi_6=\widetilde{\mathcal{A}}\exp(-\mathcal{G})$ and $\phi_7=\left(\gamma_{\mathrm{I}}\widetilde{\mathcal{C}}\right)^{-\delta}$ are independent of ξ, while the Pcov depends on ξ via $\mathcal{B}(\xi)=\sigma^2\gamma_{\mathrm{D}}\xi^{-1}$. Taking the first-order derivative of (20) with respect to ξ we have

$$\begin{aligned}&\dot{\widetilde{\mathcal{P}}}(\xi)\\ &= -\delta\phi_4\phi_5\dot{\mathcal{B}}(\xi)\left(\mathcal{B}(\xi)\right)^{-\delta-1}\exp\left(-\phi_5(\mathcal{B}(\xi))^{-\delta}\right)\\ &\quad\times\mathbf{1}\left(\mathcal{B}(\xi)-\gamma_{\mathrm{I}}\widetilde{\mathcal{C}}\right)\\ &\quad-\delta\phi_6\dot{\mathcal{B}}(\xi)\left(\mathcal{B}(\xi)\right)^{-\delta-1}\mathbf{1}\left(\gamma_{\mathrm{I}}\widetilde{\mathcal{C}}-\mathcal{B}(\xi)\right)\mathbf{1}\left(\mathcal{B}(\xi)-\widetilde{\mathcal{C}}\right)\\ &= -\delta\widetilde{\mathcal{A}}\dot{\mathcal{B}}(\xi)\left(\mathcal{B}(\xi)\right)^{-\delta-1}\left[\exp\left(-(\gamma_{\mathrm{I}})^{\delta}\widetilde{\mathcal{A}}\mathcal{G}(\mathcal{B}(\xi))^{-\delta}\right)\right.\\ &\quad\times\mathbf{1}\left(\mathcal{B}(\xi)-\gamma_{\mathrm{I}}\widetilde{\mathcal{C}}\right)+\exp(-\mathcal{G})\mathbf{1}\left(\gamma_{\mathrm{I}}\widetilde{\mathcal{C}}-\mathcal{B}(\xi)\right)\\ &\quad\left.\times\mathbf{1}\left(\mathcal{B}(\xi)-\widetilde{\mathcal{C}}\right)\right]\geq 0,\quad\forall\xi\geq 0,\end{aligned}\tag{21}$$

where $\dot{\mathcal{B}}(\xi)=-\sigma^2\gamma_{\mathrm{D}}\xi^{-2}\leq 0$. The second-order derivative of Pcov is then computed, in order to prove the concavity of the function in (22), as shown at the bottom of the next page. Here $\mathcal{T}_{21}(\xi)=\ddot{\mathcal{B}}(\xi)\mathcal{B}(\xi)-(\delta+1)\left(\dot{\mathcal{B}}(\xi)\right)^2=\left(\sigma^2\gamma_{\mathrm{D}}\xi^{-2}\right)^2[2-(\delta+1)]\geq 0$, and $\delta<1$, since $\beta>2$. From (22) it is evinced that the coverage probability Pcov is a concave function of the transmit power P_{tx}. The equality in (22) holds only for $\xi\to\infty$ and is given in (23), as shown at the bottom of the next page. Since $\ddot{\widetilde{\mathcal{P}}}(\xi)$ is a negative function for $\xi<\infty$, $\dot{\widetilde{\mathcal{P}}}(\xi)$ is a monotonically decreasing function of ξ and attains its minimum for $\xi\to\infty$ and is given by (24), as shown at the bottom of the next page. Since $\dot{\widetilde{\mathcal{P}}}(\xi)$ is a monotonically decreasing function, from (21) and (24), it holds that $\dot{\widetilde{\mathcal{P}}}(\xi)$ is strictly positive and becomes equal to 0 only for $\xi\to\infty$. Hence, $\widetilde{\mathcal{P}}(\xi)$ is a concave monotonically increasing function of ξ. Finally, the asymptotic behavior of $\widetilde{\mathcal{P}}(\xi)$ when $\xi\to 0$ and when $\xi\to+\infty$ is computed directly from (20) since $\mathcal{B}(\xi\to 0)=+\infty$ and $\mathcal{B}(\xi\to+\infty)=0$, respectively. QED.

Appendix F
Proof of Proposition 4

In this appendix, we prove that Pcov is neither jointly convex nor jointly concave with respect to both the ED density and the transmit power. Moreover, we evince that no joint optimum pair of ω and ξ exists, jointly maximizing the Pcov. We commence by rewriting Pcov in (25), as shown at the bottom of the next page. The Hessian matrix and the Hessian determinant of $\widetilde{\mathcal{P}}(\omega,\xi)$ are then given by

$$H_{\widetilde{\mathcal{P}}}(\omega,\xi)=\begin{bmatrix}\frac{\partial^2\widetilde{\mathcal{P}}(\omega,\xi)}{\partial^2\omega} & \frac{\partial^2\widetilde{\mathcal{P}}(\omega,\xi)}{\partial\omega\partial\xi}\\ \frac{\partial^2\widetilde{\mathcal{P}}(\omega,\xi)}{\partial\xi\partial\omega} & \frac{\partial^2\widetilde{\mathcal{P}}(\omega,\xi)}{\partial^2\xi}\end{bmatrix},$$

$$\begin{aligned}\mathrm{Det}\left\{H_{\widetilde{\mathcal{P}}}(\omega,\xi)\right\} &= \frac{\partial^2\widetilde{\mathcal{P}}(\omega,\xi)}{\partial^2\omega}\frac{\partial^2\widetilde{\mathcal{P}}(\omega,\xi)}{\partial^2\xi}\\ &\quad-\left(\frac{\partial^2\widetilde{\mathcal{P}}(\omega,\xi)}{\partial\omega\partial\xi}\right)^2<0,\end{aligned}\tag{26}$$

where (26) holds for $\omega < \infty, \xi < \infty$, since according to Propositions 2, $\partial^2\widetilde{\mathcal{P}}(\omega,\xi)/\partial^2\omega > 0$, for $\omega < \infty$ and according to Proposition 3, $\partial^2\widetilde{\mathcal{P}}(\omega,\xi)/\partial^2\xi < 0$, for $\xi < \infty$.

Since $H_{\widetilde{\mathcal{P}}}(\omega,\xi)$ has only 2 arguments (i.e. ω and ξ), the determinant $\mathrm{Det}\{H_{\widetilde{\mathcal{P}}}(\omega,\xi)\}$ is equal to the product of the eigenvalues of $H_{\widetilde{\mathcal{P}}}(\omega,\xi)$. Hence, since the product of the eigenvalues is negative, the eigenvalues are of opposite sign and the Hessian is neither positive semi-definite nor negative semi-definite. Pcov is therefore neither jointly convex nor jointly concave. Moreover, according to the second partial derivative test, since $\mathrm{Det}\{H_{\widetilde{\mathcal{P}}}(\omega,\xi)\} < 0$, then even if $\frac{\partial\widetilde{\mathcal{P}}(\omega,\xi)}{\partial\omega} = \frac{\partial\widetilde{\mathcal{P}}(\omega,\xi)}{\partial\xi} = 0$ at (ω_0, ξ_0), then (ω_0, ξ_0) is only a saddle point. Hence, no global optimum (ω, ξ) exists, that jointly maximizes the Pcov, and as a result the standalone approaches of Propositions 2 and 3 can be followed for the standalone optimization of ω and ξ respectively. QED.

Appendix G
Proof of Proposition 5

Let us first define the $\widetilde{\mathrm{ASE}_{k,s}}$ as a function of ω as follows

$$\widetilde{\mathrm{ASE}_{k,s}} = \widetilde{\mathcal{S}}(\omega=\lambda) = \lambda^{\mathcal{A}}\widetilde{\mathcal{RP}_{\mathrm{cov}}}(\gamma_{\mathrm{D}}, s) = \phi_8\mathcal{G}(\omega)\widetilde{\mathcal{P}}(\omega), \quad (27)$$

where $\phi_8 = \mathcal{R}/(\pi R^2)$. Taking the first-order derivative of $\widetilde{\mathcal{S}}(\omega)$ with respect to ω we have

$$\begin{aligned}\dot{\widetilde{\mathcal{S}}}(\omega)/\phi_8 &= d\widetilde{\mathcal{S}}(\omega)/d\omega = \dot{\mathcal{G}}(\omega)\widetilde{\mathcal{P}}(\omega) + \mathcal{G}(\omega)\dot{\widetilde{\mathcal{P}}}(\omega)\\ &= \phi_1\phi_2\dot{\mathcal{G}}(\omega)\exp(-\phi_2\mathcal{G}(\omega)) + \phi_3\dot{\mathcal{G}}(\omega)(1-\mathcal{G}(\omega))\\ &\quad\times\exp(-\mathcal{G}(\omega))\mathbf{1}\left(\gamma_{\mathrm{I}}\widetilde{\mathcal{C}} - \mathcal{B}\right). \end{aligned} \quad (28)$$

Here, the constant term ϕ_8 has been moved to the left hand side of (28) to simplify the notation in the analysis. From (28) the following conclusions hold: i) if $\mathcal{B} \geq \gamma_{\mathrm{I}}\widetilde{\mathcal{C}}$, then $\dot{\widetilde{\mathcal{S}}}(\omega) > 0$ if $\omega < \infty$ and $\dot{\widetilde{\mathcal{S}}}(\omega) = 0$ if $\omega \to \infty$. ii) if $\mathcal{B} < \gamma_{\mathrm{I}}\widetilde{\mathcal{C}}$ then $\phi_2 = 1$ and (28) is rewritten as follows

$$\dot{\widetilde{\mathcal{S}}}(\omega) = \dot{\mathcal{G}}(\omega)(\phi_1 + \phi_3 - \phi_3\mathcal{G}(\omega))\exp(-\mathcal{G}(\omega)). \quad (29)$$

From (29), the root of $\dot{\mathcal{S}}(\omega)$, is given by $\omega^* = \left(\rho^A\pi R^2\right)^{-1}(1+\phi_1/\phi_3)$.

Now the convexity or concavity of the ASE is examined by computing the second-order derivative of $\mathcal{S}(\omega)$ and is given by (30), as shown at the bottom of the next page, where again the constant term ϕ_8, has been moved to the left hand side of

$$\begin{aligned}\ddot{\widetilde{\mathcal{P}}}(\xi) &= -\delta\phi_4\phi_5\exp\left(-\phi_5(\mathcal{B}(\xi))^{-\delta}\right)\mathbf{1}\left(\mathcal{B}(\xi) - \gamma_{\mathrm{I}}\widetilde{\mathcal{C}}\right)\\ &\quad\times\left(\ddot{\mathcal{B}}(\xi)(\mathcal{B}(\xi))^{-\delta-1} - (\delta+1)\left[\dot{\mathcal{B}}(\xi)\right]^2(\mathcal{B}(\xi))^{-\delta-2} + \phi_5\delta\left[\dot{\mathcal{B}}(\xi)(\mathcal{B}(\xi))^{-\delta-1}\right]^2\right)\\ &\quad-\delta\phi_6\mathbf{1}\left(\mathcal{B}(\xi) - \widetilde{\mathcal{C}}\right)\left(\ddot{\mathcal{B}}(\xi)(\mathcal{B}(\xi))^{-\delta-1} - (\delta+1)\left[\dot{\mathcal{B}}(\xi)\right]^2(\mathcal{B}(\xi))^{-\delta-2}\right)\mathbf{1}\left(\gamma_{\mathrm{I}}\widetilde{\mathcal{C}} - \mathcal{B}_k(\xi)\right)\\ &= -\delta\phi_4\phi_5\exp\left(-\phi_5(\mathcal{B}(\xi))^{-\delta}\right)\\ &\quad\times\left((\mathcal{B}(\xi))^{-\delta-2}\mathcal{T}_{21}(\xi) + \phi_5\delta\left[\dot{\mathcal{B}}(\xi)(\mathcal{B}(\xi))^{-\delta-1}\right]^2\right)\mathbf{1}\left(\mathcal{B}(\xi) - \gamma_{\mathrm{I}}\widetilde{\mathcal{C}}\right) - \delta\phi_6(\mathcal{B}(\xi))^{-\delta-1}\mathcal{T}_{21}(\xi)\\ &\quad\times\mathbf{1}\left(\gamma_{\mathrm{I}}\widetilde{\mathcal{C}} - \mathcal{B}(\xi)\right)\mathbf{1}\left(\mathcal{B}(\xi) - \widetilde{\mathcal{C}}\right) \leq 0, \end{aligned} \quad (22)$$

$$\begin{aligned}\ddot{\widetilde{\mathcal{P}}}(\xi\to\infty) &= -\delta\phi_4\phi_5\exp\left(-\phi_5(\mathcal{B}(\xi))^{-\delta}\right)\left((\mathcal{B}(\xi))^{-\delta-2}\mathcal{T}_{21}(\xi) + \phi_5\delta\left[\dot{\mathcal{B}}(\xi)(\mathcal{B}(\xi=\infty))^{-\delta-1}\right]^2\right)\\ &\quad\times\underbrace{\mathbf{1}\left(\mathcal{B}(\xi=\infty) - \gamma_{\mathrm{I}}\widetilde{\mathcal{C}}\right)}_{\to 0} - \delta\phi_6(\mathcal{B}(\xi))^{-\delta-1}\mathcal{T}_{21}(\xi)\mathbf{1}\left(\gamma_{\mathrm{I}}\widetilde{\mathcal{C}} - \mathcal{B}(\xi)\right)\underbrace{\mathbf{1}\left(\mathcal{B}(\xi) - \widetilde{\mathcal{C}}\right)}_{\to 0} = 0. \end{aligned} \quad (23)$$

$$\begin{aligned}\dot{\widetilde{\mathcal{P}}}(\xi\to\infty) &= -\delta\widetilde{\mathcal{A}}\dot{\mathcal{B}}(\xi)(\mathcal{B}(\xi))^{-\delta-1}\left[\exp\left(-(\gamma_{\mathrm{I}})^{\delta}\widetilde{\mathcal{A}}\mathcal{G}(\mathcal{B}(\xi))^{-\delta}\right)\underbrace{\mathbf{1}\left(\mathcal{B}(\xi) - \gamma_{\mathrm{I}}\widetilde{\mathcal{C}}\right)}_{=0} + \exp(-\mathcal{G})\mathbf{1}\left(\gamma_{\mathrm{I}}\widetilde{\mathcal{C}} - \mathcal{B}(\xi)\right)\underbrace{\mathbf{1}\left(\mathcal{B}(\xi) - \widetilde{\mathcal{C}}\right)}_{=0}\right]\\ &= 0. \end{aligned} \quad (24)$$

$$\begin{aligned}\widetilde{\mathcal{P}}(\omega,\xi) &= (\gamma_{\mathrm{I}})^{-\delta}(\mathcal{G}(\omega))^{-1}\left(1 - \exp\left(-\widetilde{\mathcal{A}}\mathcal{G}(\omega)(\gamma_{\mathrm{I}})^{\delta}\left(\max\left\{\mathcal{B}(\xi), \gamma_{\mathrm{I}}\widetilde{\mathcal{C}}\right\}^{-\delta}\right)\right)\right)\\ &\quad+\widetilde{\mathcal{A}}\exp(-\mathcal{G}(\omega))\left(\max\left\{\mathcal{B}(\xi), \widetilde{\mathcal{C}}\right\}^{-\delta} - \left(\gamma_{\mathrm{I}}\widetilde{\mathcal{C}}\right)^{-\delta}\right)\mathbf{1}\left(\gamma_{\mathrm{I}}\widetilde{\mathcal{C}} - \mathcal{B}(\xi)\right). \end{aligned} \quad (25)$$

the equation to simplify the notation. Focusing again on the first case study where i) $\mathcal{B} \geq \gamma_I \widetilde{\mathcal{C}}$, (30) can be rewritten as follows

$$\ddot{\widetilde{\mathcal{S}}}(\omega) = \phi_8 \left[-\phi_1 \dot{\mathcal{G}}(\omega) (\phi_2)^2 \exp(-\phi_2 \mathcal{G}(\omega)) \right] \leq 0. \quad (31)$$

As a result, in this first case the ASE is a concave function of ω. Subsequently focusing on the second case where ii) $\mathcal{B} < \gamma_I \widetilde{\mathcal{C}}$, then (30) can be rewritten as follows

$$\ddot{\widetilde{\mathcal{S}}}(\omega) = -\dot{\mathcal{G}}(\omega) \exp(-\mathcal{G}(\omega)) (\phi_1 + \phi_3 (2 - \mathcal{G}(\omega))). \quad (32)$$

The inflection point of (32) is given by $\omega^{**} = \left(\rho^A \pi R^2\right)^{-1} (2 + \phi_1/\phi_3)$, and $\widetilde{\mathcal{S}}(\omega)$ is a concave function for $\omega < \omega^{**}$ and a convex function otherwise.

Subsequently, in order to study the asymptotic behavior of $\widetilde{\mathcal{S}}(\omega)$ when ω goes to either zero or infinity, we rewrite the ASE as follows

$$\widetilde{\mathcal{S}}(\omega) = \phi_8 \phi_1 (1 - \exp(-\phi_2 \mathcal{G}(\omega))) + \phi_8 \phi_3 \mathcal{G}(\omega) \times \exp(-\mathcal{G}(\omega)) \mathbf{1}\left(\gamma_{\mathrm{I}} \widetilde{\mathcal{C}} - \mathcal{B}\right). \quad (33)$$

Based on (33) it straightforwardly holds that when $\omega \to 0 \Rightarrow \widetilde{\mathcal{S}}(\omega) \to 0$ and when $\omega \to \infty$, it holds that

$$\begin{aligned} \lim_{\omega \to \infty} \left(\widetilde{\mathcal{S}}(\omega)\right) &= \phi_8 (\phi_1 + \phi_3) = \lim_{\omega \to \infty} \left(\frac{\mathcal{G}(\omega)}{\exp(\mathcal{G}(\omega))} \right) \\ &\quad \times \mathbf{1}\left(\gamma_{\mathrm{I}} \widetilde{\mathcal{C}} - \mathcal{B}\right) \overset{(a)}{=} \phi_1 \phi_8 \\ &= (\gamma_{\mathrm{I}})^{-\delta} \left(\mathcal{R}/\pi R^2\right), \end{aligned} \quad (34)$$

where (a) is derived by employing L'Hospital's rule. QED.

APPENDIX H
PROOF OF COROLLARY 1

The behavior of ω^* (and ω^{**}) with respect to the path-loss exponent β is studied hereafter. Focusing on the case where i) $\widetilde{\mathcal{C}} \leq \mathcal{B} \leq \gamma_{\mathrm{I}} \widetilde{\mathcal{C}}$ and utilising the functions $\widetilde{\mathcal{A}} = \frac{1}{R^2} \left(\frac{K_0}{\mathcal{F}}\right)^{-\delta}$, $\widetilde{\mathcal{C}} = \frac{\mathcal{F}}{R^\beta K_0}$ and $\delta(\beta) = 2/\beta$, $\upsilon(x)$ of Proposition 5 is rewritten as

$$\upsilon(\beta; x) = \left(p^A \pi R^2\right)^{-1} \left(x + R^2 \left(K_0 / (\gamma_{\mathrm{I}} \mathcal{F})^{-1} \right)^{\delta(\beta)} \times \left((\mathcal{B})^{-\delta(\beta)} - (\gamma_I)^{-\delta(\beta)} \right)^{-1} \right). \quad (35)$$

Taking the first-order derivative of (35) with respect to β we have

$$\dot{\upsilon}(\beta; x) = (2/\beta^2) R^2 (K_0/\mathcal{F})^{\delta(\beta)} \left((\mathcal{B})^{-\delta(\beta)} - (\gamma_{\mathrm{I}})^{-\delta(\beta)} \right)^{-2} \times \mathcal{T}_{33}(K_0/\mathcal{F}, \gamma_{\mathrm{I}}/\mathcal{B}, \delta) \quad (36)$$

where $\mathcal{T}_{33}\left(\frac{K_0}{\mathcal{F}}, \frac{\gamma_{\mathrm{I}}}{\mathcal{B}}, \delta\right) = \left[\log\left(\frac{K_0}{\mathcal{F}}\right) - \left(\frac{\gamma_{\mathrm{I}}}{\mathcal{B}}\right)^{\delta(\beta)} \log\left(\frac{\mathcal{B} K_0}{\gamma_{\mathrm{I}} \mathcal{F}}\right) \right]$. Hence, in order to examine the sign of (36) the sign of $\mathcal{T}_{33}\left(\frac{K_0}{\mathcal{F}}, \frac{\gamma_{\mathrm{I}}}{\mathcal{B}}, \delta\right)$ needs to be examined first. Recalling that $\delta \in (0, 1)$, $\mathcal{T}_{33}\left(\frac{K_0}{\mathcal{F}}, \frac{\gamma_{\mathrm{I}}}{\mathcal{B}}, \delta\right)$ has the following properties:

$$\begin{cases} 0 \leq \ln\left(\frac{K_0}{\mathcal{F}}\right) - \ln\left(\frac{\mathcal{B} K_0}{\gamma_{\mathrm{I}} \mathcal{F}}\right) \leq \mathcal{T}_{33}\left(\frac{K_0}{\mathcal{F}}, \frac{\gamma_{\mathrm{I}}}{\mathcal{B}}, \delta\right) \\ \quad \frac{K_0}{\mathcal{F}} < \frac{\mathcal{B}}{\gamma_{\mathrm{I}}} \\ \ln\left(\frac{K_0}{\mathcal{F}}\right) - \frac{\mathcal{B}}{\gamma_{\mathrm{I}}} \ln\left(\frac{\mathcal{B} K_0}{\gamma_{\mathrm{I}} \mathcal{F}}\right) \leq \mathcal{T}_{33}\left(\frac{K_0}{\mathcal{F}}, \frac{\gamma_{\mathrm{I}}}{\mathcal{B}}, \delta\right) \\ \quad \frac{K_0}{\mathcal{F}} \geq \frac{\mathcal{B}}{\gamma_{\mathrm{I}}}. \end{cases} \quad (37)$$

Hence, $\mathcal{T}_{33}\left(\frac{K_0}{\mathcal{F}}, \frac{\gamma_{\mathrm{I}}}{\mathcal{B}}, \delta\right)$ is always non-negative if $\ln\left(\frac{K_0}{\mathcal{F}}\right) - \frac{\mathcal{B}}{\gamma_{\mathrm{I}}} \ln\left(\frac{\mathcal{B} K_0}{\gamma_{\mathrm{I}} \mathcal{F}}\right) \geq 0 \Leftrightarrow \mathcal{F} \geq K_0 \exp\left(-\frac{\log(\gamma_{\mathrm{I}}/\mathcal{B})}{1 - (\gamma_{\mathrm{I}}/\mathcal{B})^{-1}}\right)$.

Subsequently, focusing on the second case where ii) $\widetilde{\mathcal{C}} > \mathcal{B}$ and taking the first-order derivative of ω^* with respect to β we obtain

$$\begin{aligned} &\dot{\upsilon}(\beta; x) \\ &= \frac{2}{\beta^2} R^2 \left(\frac{K_0}{\gamma_{\mathrm{I}} \mathcal{F}}\right)^{\delta(\beta)} \left(1 - (\gamma_{\mathrm{I}})^{-\delta(\beta)}\right)^{-2} \\ &\quad \times \left[(\gamma_{\mathrm{I}})^{-\delta(\beta)} \log(\gamma_{\mathrm{I}}) - \log\left(\frac{K_0}{\gamma_{\mathrm{I}} \mathcal{F}}\right) \left(1 - (\gamma_{\mathrm{I}})^{-\delta(\beta)}\right) \right] \\ &= \frac{2}{\beta^2} R^2 \left(\frac{K_0}{\mathcal{F}}\right)^{\delta(\beta)} \left(1 - (\gamma_{\mathrm{I}})^{-\delta(\beta)}\right)^{-2} \mathcal{T}_{33}\left(\frac{K_0}{\mathcal{F}}, \gamma_{\mathrm{I}}, \delta\right). \end{aligned} \quad (38)$$

From (38) it is demonstrated that $\dot{\upsilon}(\beta; x)$ has a similar behaviour as (36), and therefore $\dot{\upsilon}(\beta; x)$ is again non-negative if $\mathcal{F} \geq K_0 \exp\left(-\frac{\log(\gamma_{\mathrm{I}})}{1 - (\gamma_{\mathrm{I}})^{-1}}\right)$. Hence, for both cases (i.e. i and ii) $\upsilon(x)$ is an increasing function of β provided that the following unified condition holds $\mathcal{F} \geq K_0 \exp\left(-\frac{\log(\gamma_{\mathrm{I}}/\upsilon)}{1 - (\gamma_{\mathrm{I}}/\upsilon)^{-1}}\right)$ where $\upsilon = \mathcal{B}$ if $\widetilde{\mathcal{C}} \leq \mathcal{B} \leq \gamma_{\mathrm{I}} \widetilde{\mathcal{C}}$ and respectively $\upsilon = 1$ if $\widetilde{\mathcal{C}} > \mathcal{B}$. This concludes the proof.

APPENDIX I
PROOF OF PROPOSITION 7

Following the same steps as in Proposition 4, the Hessian matrix and the Hessian determinant of $\widetilde{\mathcal{S}}(\omega, \xi)$ are given by

$$H_{\widetilde{\mathcal{S}}}(\omega, \xi) = \begin{bmatrix} \frac{\partial^2 \widetilde{\mathcal{S}}(\omega,\xi)}{\partial^2 \omega} & \frac{\partial^2 \widetilde{\mathcal{S}}(\omega,\xi)}{\partial \omega \partial \xi} \\ \frac{\partial^2 \widetilde{\mathcal{S}}(\omega,\xi)}{\partial \xi \partial \omega} & \frac{\partial^2 \widetilde{\mathcal{S}}(\omega,\xi)}{\partial^2 \xi} \end{bmatrix}$$

$$\mathrm{Det}\left\{H_{\widetilde{\mathcal{S}}}(\omega, \xi)\right\} = \frac{\partial^2 \widetilde{\mathcal{S}}(\omega, \xi)}{\partial^2 \omega} \frac{\partial^2 \widetilde{\mathcal{S}}(\omega, \xi)}{\partial^2 \xi}$$

$$\begin{aligned} \ddot{\widetilde{\mathcal{S}}}(\omega)/\phi_8 &= 2\dot{\mathcal{G}}(\omega) \dot{\widetilde{\mathcal{P}}}(\omega) + \mathcal{G}(\omega) \ddot{\widetilde{\mathcal{P}}}(\omega) = \rho^A \pi R^2 \left(2\dot{\widetilde{\mathcal{P}}}(\omega) + \omega \ddot{\widetilde{\mathcal{P}}}(\omega)\right) \\ &= -2\phi_1 \dot{\mathcal{G}}(\omega) (\mathcal{G}(\omega))^{-2} [1 - \exp(-\phi_2 \mathcal{G}(\omega)) (1 + \phi_2 \mathcal{G}(\omega))] \\ &\quad + \left[-2\phi_3 \dot{\mathcal{G}}(\omega) \exp(-\mathcal{G}(\omega)) + \phi_3 \dot{\mathcal{G}}(\omega) \mathcal{G}(\omega) \exp(-\mathcal{G}(\omega)) \right] \\ &\quad \times \mathbf{1}\left(\gamma_I \widetilde{\mathcal{C}} - \mathcal{B}\right) + \phi_1 \dot{\mathcal{G}}(\omega) (\mathcal{G}(\omega))^{-2} \left(2 - \exp(-\phi_2 \mathcal{G}(\omega)) \left(1 + (1 + \phi_2 \mathcal{G}(\omega))^2\right)\right), \end{aligned} \quad (30)$$

$$- \left(\frac{\partial^2 \widetilde{\mathcal{S}}(\omega,\xi)}{\partial\omega\partial\xi} \right)^2. \tag{39}$$

From Propositions 5 and 6, we have $\frac{\partial^2 \widetilde{\mathcal{S}}(\omega,\xi)}{\partial^2\omega} = -\rho^A \pi R^2 \phi_8 \phi_1 \dot{\mathcal{G}}(\omega) (\phi_2)^2 \exp(-\phi_2 \mathcal{G}(\omega)) \leq 0$ when $\gamma_{\mathrm{I}}\widetilde{\mathcal{C}} \leq \mathcal{B}$; $\frac{\partial^2 \widetilde{\mathcal{S}}(\omega,\xi)}{\partial^2\omega} = -\rho^A \pi R^2 \phi_8 \dot{\mathcal{G}}(\omega) \exp(-\mathcal{G}(\omega)) (\phi_1 + \phi_3 (2 - \mathcal{G}(\omega)))$ when $\gamma_{\mathrm{I}}\widetilde{\mathcal{C}} > \mathcal{B}$; and $\frac{\partial^2 \widetilde{\mathcal{S}}(\omega,\xi)}{\partial^2\xi} \leq 0$ when $\widetilde{\mathcal{C}} \leq \mathcal{B}$ and $\frac{\partial^2 \widetilde{\mathcal{S}}(\omega,\xi)}{\partial^2\xi} = 0$ when $\widetilde{\mathcal{C}} > \mathcal{B}$. Hence, as opposed to the coverage probability that is characterized by a common universal behavior over the whole domain (i.e. being neither jointly convex nor jointly concave) the ASE is not characterized by a common universal behavior over the whole domain. That is, since the Hessian determinant takes both negative and positive values which asserts that there are indeed regions where the ASE is neither jointly convex nor joinlty concave and other regions where the same behaviour is exhibited with respect to both parameters ω and ξ. Since the ASE is not characterized by a common behaviour, the analysis focuses on examining whether a global joint optimum exist maximizing the ASE over both ω and ξ.

In this course, we depart from (29) and its root ω^* and examine whether the first derivative $\dot{\widetilde{\mathcal{S}}}_\xi(\omega^*,\xi)$ with respect to ξ becomes equal to zero. We commence by defining $\dot{\widetilde{\mathcal{S}}}_\xi(\omega^*,\xi)$ which is given by (40), as shown at the bottom of the page.

Here $\phi_1 = (\gamma_{\mathrm{I}})^{-\delta}$ and $\phi_3 = \widetilde{\mathcal{A}}\left(\left(\max\left\{ \widetilde{\mathcal{C}}, \mathcal{B} \right\} \right)^{-\delta} - \left(\gamma_{\mathrm{I}}\widetilde{\mathcal{C}} \right)^{-\delta} \right)$.

From (40), three different behaviours of $\dot{\widetilde{\mathcal{S}}}_\xi(\omega^*,\xi)$ arise. In particular:

i) If $\mathcal{B}(\xi) \geq \gamma_{\mathrm{I}}\mathcal{C} > \mathcal{C} : (\mathcal{B}(\xi))^{-\delta} - (\gamma_{\mathrm{I}}\mathcal{C})^{-\delta} < 0$, then we obtain (41), as shown at the bottom of the page.

And solving for the root ξ^* we obtain $\dot{\widetilde{\mathcal{S}}}_\xi(\omega^*,\xi^*) = 0 \Rightarrow \xi^* = 0$ as a possible solution that corresponds to an indeterminate case and for which the limit $\dot{\widetilde{\mathcal{S}}}(\omega^*,\xi \to 0)$ needs to be computed. Since the considered range is $\mathcal{B}(\xi) \geq \gamma_{\mathrm{I}}\mathcal{C} \Leftrightarrow \sigma^2\gamma_{\mathrm{D}}\xi^{-1} \geq \gamma_{\mathrm{I}}\mathcal{C} \Leftrightarrow \xi \leq \frac{\sigma^2\gamma_{\mathrm{D}}}{\gamma_{\mathrm{I}}\mathcal{C}}$ then $\xi^* = 0$ is indeed a possible solution within this range. However, by definition the case $P_{\mathrm{tx}} = 0$ is a minimum of the ASE and not a maximum. Hence, we proceed with the analysis.

$$\begin{aligned}
\dot{\widetilde{\mathcal{S}}}_\xi(\omega^*,\xi) = {} & -\phi_8 \mathcal{G}(\omega^*) \delta \widetilde{\mathcal{A}} \dot{\mathcal{B}}(\xi) (\mathcal{B}(\xi))^{-\delta-1} \Big[\exp\left(-(\gamma_{\mathrm{I}})^\delta \widetilde{\mathcal{A}} \mathcal{G}(\omega^*) (\mathcal{B}(\xi))^{-\delta} \right) \mathbf{1}\left(\mathcal{B}(\xi) - \gamma_{\mathrm{I}}\widetilde{\mathcal{C}} \right) \\
& + \exp(-\mathcal{G}(\omega^*)) \mathbf{1}\left(\gamma_{\mathrm{I}}\widetilde{\mathcal{C}} - \mathcal{B}(\xi) \right) \\
& \times \mathbf{1}\left(\mathcal{B}(\xi) - \widetilde{\mathcal{C}} \right) \Big] = \phi_8 (1 + \phi_1/\phi_3) \delta \widetilde{\mathcal{A}} \dot{\mathcal{B}}(\xi) (\mathcal{B}(\xi))^{-\delta-1} \Big[\exp\left(-(\gamma_{\mathrm{I}})^\delta \widetilde{\mathcal{A}} (1 + \phi_1/\phi_3) (\mathcal{B}(\xi))^{-\delta} \right) \\
& \times \mathbf{1}\left(\mathcal{B}(\xi) - \gamma_{\mathrm{I}}\widetilde{\mathcal{C}} \right) + \exp((1 + \phi_1/\phi_3)) \mathbf{1}\left(\gamma_{\mathrm{I}}\widetilde{\mathcal{C}} - \mathcal{B}(\xi) \right) \mathbf{1}\left(\mathcal{B}(\xi) - \widetilde{\mathcal{C}} \right) \Big],
\end{aligned} \tag{40}$$

$$\begin{aligned}
\dot{\widetilde{\mathcal{S}}}_\xi(\omega^*,\xi) = {} & \phi_8 \delta \left(\mathcal{A} - (\gamma_{\mathrm{I}})^{-\delta} \left((\gamma_{\mathrm{I}}\mathcal{C})^{-\delta} - (\mathcal{B}(\xi))^{-\delta} \right)^{-1} \right) \left(\dot{\mathcal{B}}(\xi) \right) (\mathcal{B}(\xi))^{-\delta-1} \\
& \times \exp\left(-(\gamma_{\mathrm{I}})^\delta \left(\mathcal{A} - (\gamma_{\mathrm{I}})^{-\delta} \left((\gamma_{\mathrm{I}}\mathcal{C})^{-\delta} - (\mathcal{B}(\xi))^{-\delta} \right)^{-1} \right) (\mathcal{B}(\xi))^{-\delta} \right)
\end{aligned} \tag{41}$$

$$\begin{aligned}
\dot{\widetilde{\mathcal{S}}}_\xi(\omega^*,\xi) = {} & \phi_8 \delta \left(\mathcal{A} + \phi_1 \left((\mathcal{C})^{-\delta} - (\gamma_{\mathrm{I}}\mathcal{C})^{-\delta} \right)^{-1} \right) (\mathcal{B}(\xi))^{+} (\mathcal{B}(\xi))^{-\delta-1} \\
& \times \Bigg[\exp\left(-(\gamma_{\mathrm{I}})^\delta \left(\mathcal{A} + \phi_1 \left((\mathcal{C})^{-\delta} - (\gamma_{\mathrm{I}}\mathcal{C})^{-\delta} \right)^{-1} \right) (\mathcal{B}(\xi))^{-\delta} \right) \\
& \times \underbrace{\mathbf{1}(\mathcal{B}(\xi) - \gamma_{\mathrm{I}}\mathcal{C})}_{=0} + \exp\left(1 + \phi_1 \left(\mathcal{A} \left((\mathcal{C})^{-\delta} - (\gamma_{\mathrm{I}}\mathcal{C})^{-\delta} \right) \right)^{-1} \right) \mathbf{1}(\gamma_{\mathrm{I}}\mathcal{C} - \mathcal{B}(\xi)) \underbrace{\mathbf{1}(\mathcal{B}(\xi) - \mathcal{C})}_{=0} \Bigg] = 0.
\end{aligned} \tag{43}$$

$$\begin{aligned}
\eta_{1,2} &= \frac{1}{2} \left(\mathrm{Tr}\{H_{\widetilde{\mathcal{S}}}(\omega,\xi^*)\} \pm \sqrt{\left(\mathrm{Tr}\{H_{\widetilde{\mathcal{S}}}(\omega,\xi^*)\} \right)^2 - 4\mathrm{Det}\{H_{\widetilde{\mathcal{S}}}(\omega,\xi^*)\}} \right) \\
&= \begin{cases} \eta_1 = \mathrm{Tr}\{H_{\widetilde{\mathcal{S}}}(\omega,\xi^*)\} = \frac{\partial^2 \mathcal{S}(\omega,\xi^*)}{\partial^2\omega} = \frac{\partial^2 \mathcal{S}(\omega,\xi^*)}{\partial^2\omega} = \begin{cases} \eta_1 < 0 & \omega < \omega^{**} \\ \eta_1 > 0 & \omega > \omega^{**} \\ \eta_1 = 0 & \omega = \omega^{**} \end{cases} \\ \eta_2 = 0, \end{cases}
\end{aligned} \tag{47}$$

ii) If $\gamma_{\mathrm{I}}\mathcal{C} \geq \mathcal{B}(\xi) > \mathcal{C} : (\mathcal{B}(\xi))^{-\delta} - (\gamma_{\mathrm{I}}\mathcal{C})^{-\delta} \geq 0$, then we have

$$\dot{\widetilde{\mathcal{S}}}_{\xi}(\omega^*,\xi) = \phi_8\delta\left(\mathcal{A}+\phi_1\left((\mathcal{B}(\xi))^{-\delta} - (\gamma_{\mathrm{I}}\mathcal{C})^{-\delta}\right)^{-1}\right)\left(\dot{\mathcal{B}}(\xi)\right) \times (\mathcal{B}(\xi))^{-\delta-1}\exp\left(1+(\gamma_{\mathrm{I}})^{-\delta}\left(\mathcal{A}\left((\mathcal{B}(\xi))^{-\delta} - (\gamma_{\mathrm{I}}\mathcal{C})^{-\delta}\right)\right)^{-1}\right) \neq 0 \quad (42)$$

iii) If $\gamma_{\mathrm{I}}\mathcal{C} > \mathcal{C} \geq \mathcal{B}(\xi) : (\mathcal{C})^{-\delta} - (\gamma_{\mathrm{I}}\mathcal{C})^{-\delta} \geq 0$, then we have (43), as shown at the bottom of the previous page.

Hence out of the 3 cases, a joint maximum can be attained at $\mathcal{C} \geq \mathcal{B}(\xi^*) \Leftrightarrow \sigma^2\gamma_{\mathrm{D}}\xi^{*-1} \leq \mathcal{C} \Leftrightarrow \xi^* \geq \frac{\sigma^2\gamma_{\mathrm{D}}}{\mathcal{C}}$ and $\omega^* = \left(\rho^A\pi R^2\right)^{-1}(1+\phi_1/\phi_3)$ where according to (29) and (43) $\dot{\widetilde{\mathcal{S}}}_{\xi}(\omega^*,\xi^*) = \dot{\widetilde{\mathcal{S}}}_{\omega}(\omega^*,\xi^*) = 0$.

In order to determine whether $\widetilde{\mathcal{S}}(\omega^*,\xi^*)$ is indeed a maximum of the ASE, it needs to be determined whether $\widetilde{\mathcal{S}}(\omega,\xi)$ is concave at (ω^*,ξ^*). By denoting by $\eta_{1,2}$ the eigenvalues of the Hessian matrix $H_{\widetilde{\mathcal{S}}}(\omega,\xi)$, then it holds that

$$\mathrm{Det}\left\{H_{\widetilde{\mathcal{S}}}(\omega^*,\xi^*) - \eta\mathbf{I}\right\} = \eta^2 - \eta\,\mathrm{Tr}\left\{H_{\widetilde{\mathcal{S}}}(\omega^*,\xi^*)\right\} + \mathrm{Det}\left\{H_{\widetilde{\mathcal{S}}}(\omega^*,\xi^*)\right\}, \quad (44)$$

where Tr denotes the trace operator and $\mathbf{I}$ the identity matrix. Employing (44) we will hereafter examine the sign of the eigenvalues η_1,η_2 in the region of interest $\left(\omega,\xi^* = \xi \geq \frac{\sigma^2\gamma_{\mathrm{D}}}{\mathcal{C}}\right)$, to determine whether $H_{\widetilde{\mathcal{S}}}(\omega,\xi^*)$ is positive semi definite or negative semi definite. Let us derive the $\mathrm{Det}\left\{H_{\widetilde{\mathcal{S}}}(\omega,\xi^*)\right\}$ hereafter

$$\mathrm{Det}\left\{H_{\widetilde{\mathcal{S}}}(\omega,\xi^*)\right\} = \frac{\partial^2\mathcal{S}(\omega,\xi^*)}{\partial^2\omega}\frac{\partial^2\mathcal{S}(\omega,\xi^*)}{\partial^2\xi} - \left(\frac{\partial^2\mathcal{S}(\omega,\xi^*)}{\partial\omega\partial\xi}\right)^2 \quad (45)$$

where

$$\begin{aligned}
&\partial^2\mathcal{S}(\omega,\xi^*)/\partial^2\xi \\
&= -\delta\phi_4\phi_5\phi_8\mathcal{G}(\omega)\exp\left(-\phi_5(\mathcal{B}(\xi^*))^{-\delta}\right)\Big(\mathcal{T}_{21}(\xi^*) \\
&\quad\times(\mathcal{B}(\xi^*))^{-\delta-2} + \phi_5\delta\left[\left(\dot{\mathcal{B}}(\xi^*)\right)(\mathcal{B}(\xi^*))^{-\delta-1}\right]^2\Big) \\
&\quad\times\mathbf{1}(\mathcal{B}(\xi^*) - \gamma_{\mathrm{I}}\mathcal{C}) - \delta\phi_6\phi_8 \\
&\quad\times\mathcal{G}(\omega)(\mathcal{B}(\xi^*))^{-\delta-1}\mathcal{T}_{21}(\xi^*) \\
&\quad\times\mathbf{1}(\gamma_{\mathrm{I}}\mathcal{C} - \mathcal{B}(\xi^*))\,\mathbf{1}(\mathcal{B}(\xi^*) - \mathcal{C}) = 0 \\
&\partial^2\mathcal{S}(\omega,\xi^*)/\partial\omega\partial\xi \\
&= \Big[\delta\left(\dot{\mathcal{B}}(\xi^*)\right)(\mathcal{B}(\xi^*))^{-\delta-1}\mathcal{A}\left(\dot{\mathcal{G}}(\omega)\right) \\
&\quad\times\exp\left(-(\gamma_{\mathrm{I}}/\mathcal{B}(\xi^*))^{\delta}\mathcal{G}(\omega)\right)\left[(\gamma_{\mathrm{I}}/\mathcal{B}(\xi^*))^{\delta}\mathcal{A}\mathcal{G}(\omega) - 1\right]\Big] \\
&\quad\times\mathbf{1}(\mathcal{B}(\xi^*) - \gamma_{\mathrm{I}}\mathcal{C}) - \mathbf{1}(\gamma_{\mathrm{I}}\mathcal{C} - \mathcal{B}(\xi^*))\,\mathbf{1}(\mathcal{B}(\xi^*) - \mathcal{C}) \\
&\quad\times\left(\delta(\mathcal{B}(\xi^*))^{-\delta-1}\left(\dot{\mathcal{B}}(\xi^*)\right)\left(\dot{\mathcal{G}}(\omega)\right)\right. \\
&\quad\times\left.\mathcal{A}(1-\mathcal{G}(\omega))\exp(-\mathcal{G}(\omega))\right) = 0, \quad (46)
\end{aligned}$$

Which proves that $\mathrm{Det}\left\{H_{\mathcal{S}}(\omega,\xi^*)\right\} = 0$. Now, let us examine the eigenvalues of $H_{\mathcal{S}}(\omega,\xi^*)$, $\eta_{1,2}$ which is given by (47), as shown at the bottom of the previous page.

Here ω^{**} is the inflection point given in (32).

From (47), we can conclude that $H_{\widetilde{\mathcal{S}}}(\omega < \omega^{**},\xi^*)$ is negative semi definite and $H_{\widetilde{\mathcal{S}}}(\omega > \omega^{**},\xi^*)$ is positive semi definite. Thus, $\widetilde{\mathcal{S}}(\omega < \omega^{**},\xi^*)$ is concave function and $\widetilde{\mathcal{S}}(\omega > \omega^{**},\xi^*)$ is convex function. Since $\omega^* < \omega^{**}$, this means that the segment defined by $\xi^* \geq \frac{\sigma^2\gamma_{\mathrm{D}}}{\mathcal{C}}$ and $\omega^* = \left(\rho^A\pi R^2\right)^{-1}(1+\phi_1/\phi_3)$, where $\dot{\widetilde{\mathcal{S}}}_{\xi}(\omega^*,\xi^*) = \dot{\widetilde{\mathcal{S}}}_{\omega}(\omega^*,\xi^*) = 0$, lies also in a region where $\widetilde{\mathcal{S}}(\omega,\xi)$ is jointly concave (although not strictly concave) and this segment is therefore a global maximum of the ASE. QED.

ACKNOWLEDGMENT

This work was supported in part by the CPER/FEDERNUMERIC project "Intelligent Networks II" under grant agreement NUMERI06 and the H2020 MSCA IF Pathfinder project under grant agreement 891030.

REFERENCES

[1] L.-T. Tu, A. Bradai, and Y. Pousset, "A new closed-form expression of the coverage probability for different QoS in LoRa networks," in *Proc. IEEE Int. Conf. Commun. (ICC)*, Dublin, Ireland, Jun. 2020, pp. 1–6.

[2] C. Goursaud and J. M. Gorce, "Dedicated networks for IoT: PHY/MAC state of the art and challenges," *EAI Endorsed Trans. Internet Things*, vol. 1, no. 1, Oct. 2015, Art. no. 150597.

[3] L. Vangelista, "Frequency shift chirp modulation: The LoRa modulation," *IEEE Signal Process. Lett.*, vol. 24, no. 12, pp. 1818–1821, Dec. 2017.

[4] O. Georgiou and U. Raza, "Low power wide area network analysis: Can LoRa scale?" *IEEE Wireless Commun. Lett.*, vol. 6, no. 2, pp. 162–165, Apr. 2017.

[5] Z. Qin, Y. Liu, G. Y. Li, and J. A. McCann, "Performance analysis of clustered LoRa networks," *IEEE Trans. Veh. Technol.*, vol. 68, no. 8, pp. 7616–7629, Aug. 2019.

[6] A. Hoeller, Jr., R. D. Souza, O. L. A. López, H. Alves, M. de Noronha Neto, and G. Brante, "Analysis and performance optimization of LoRa networks with time and antenna diversity," *IEEE Access*, vol. 6, pp. 32820–32829, 2018.

[7] A. Mahmood, E. G. Sisinni, L. Guntupalli, R. Rondón, S. A. Hassan, and M. Gidlund, "Scalability analysis of a LoRa network under imperfect orthogonality," *IEEE Trans. Ind. Informat.*, vol. 15, no. 3, pp. 1425–1436, Mar. 2019.

[8] L. Beltramelli, A. Mahmood, P. Osterberg, and M. Gidlund, "LoRa beyond ALOHA: An investigation of alternative random access protocols," *IEEE Trans. Ind. Informat.*, vol. 17, no. 5, pp. 3544–3554, May 2021.

[9] L. Beltramelli, A. Mahmood, P. Österberg, M. Gidlund, P. Ferrari, and E. Sisinni, "Energy efficiency of slotted LoRaWAN communication with out-of-band synchronization," *IEEE Trans. Instrum. Meas.*, vol. 70, pp. 1–11, 2021.

[10] L.-T. Tu, A. Bradai, Y. Pousset, and A. I. Aravanis, "Energy efficiency analysis of LoRa networks," *IEEE Wireless Commun. Lett.*, vol. 10, no. 9, pp. 1881–1885, Sep. 2021.

[11] B. Reynders, W. Meert, and S. Pollin, "Power and spreading factor control in low power wide area networks," in *Proc. IEEE Int. Conf. Commun. (ICC)*, Paris, France, May 2017, pp. 1–6.

[12] K. Q. Abdelfadeel, V. Cionca, and D. Pesch, "Fair adaptive data rate allocation and power control in LoRaWAN," in *Proc. IEEE 19th Int. Symp. World Wireless, Mobile Multimedia Netw. (WoWMoM)*, Chania, Greece, Jun. 2018, pp. 14–15.

[13] B. Su, Z. Qin, and Q. Ni, "Energy efficient resource allocation for uplink LoRa networks," in *Proc. IEEE Global Commun. Conf. (GLOBECOM)*, Abu Dhabi, United Arab Emirates, Dec. 2018, pp. 1–7.

[14] R. B. Sørensen, D. M. Kim, J. J. Nielsen, and P. Popovski, "Analysis of latency and MAC-layer performance for class a LoRaWAN," *IEEE Wireless Commun. Lett.*, vol. 6, no. 5, pp. 566–569, Oct. 2017.

[15] J. Lyu, D. Yu, and L. Fu, "Analysis and optimization for large-scale LoRa networks: Throughput fairness and scalability," *IEEE Internet Things J.*, early access, Nov. 15, 2021, doi: 10.1109/JIOT.2021.3126600.

[16] R. Fernandes, R. Oliveira, M. Luís, and S. Sargento, "On the real capacity of LoRa networks: The impact of non-destructive communications," *IEEE Commun. Lett.*, vol. 23, no. 12, pp. 2437–2441, Dec. 2019.

[17] D. Croce, M. Gucciardo, S. Mangione, G. Santaromita, and I. Tinnirello, "Impact of LoRa imperfect orthogonality: Analysis of link-level performance," *IEEE Commun. Lett.*, vol. 22, no. 4, pp. 796–799, Apr. 2018.
[18] T. T. Lam and M. Di Renzo, "On the energy efficiency of heterogeneous cellular networks with renewable energy sources—A stochastic geometry framework," *IEEE Trans. Wireless Commun.*, vol. 19, no. 10, pp. 6752–6770, Oct. 2020.
[19] J. Haxhibeqiri, I. Moerman, J. Hoebeke, and F. Van den Abeele, "LoRa scalability: A simulation model based on interference measurements," *Sensors*, vol. 17, no. 6, p. 1193, May 2017.
[20] M. Di Renzo, T. T. Lam, A. Zappone, and M. Debbah, "A tractable closed-form expression of the coverage probability in Poisson cellular networks," *IEEE Wireless Commun. Lett.*, vol. 8, no. 1, pp. 249–252, Feb. 2019.
[21] R. Marini, W. Cerroni, and C. Buratti, "A novel collision-aware adaptive data rate algorithm for LoRaWAN networks," *IEEE Internet Things J.*, vol. 8, no. 4, pp. 2670–2680, Feb. 2021.
[22] M. Di Renzo, A. Zappone, T. T. Lam, and M. Debbah, "System-level modeling and optimization of the energy efficiency in cellular networks—A stochastic geometry framework," *IEEE Trans. Wireless Commun.*, vol. 17, no. 4, pp. 2539–2556, Apr. 2018.
[23] N. Sorni, M. Luis, T. Eirich, T. Kramp, and O. Hersent, "LoRaWAN 1201 specification," LoRa Alliance, San Ramon, CA, USA, Tech. Rep., Version 1.0, Jan. 2015.
[24] *IEEE 802.16p Machine to Machine (M2M) Evaluation Methodology Document (EMD)*, Standard IEEE 802.16p-11/0014. Accessed: Nov. 25, 2021. [Online]. Available: http://ieee802.org/16/m2m/index.html
[25] W. Xu, J. Y. Kim, W. Huang, S. S. Kanhere, S. K. Jha, and W. Hu, "Measurement, characterization, and modeling of LoRa technology in multifloor buildings," *IEEE Internet Things J.*, vol. 7, no. 1, pp. 298–310, Jan. 2020.
[26] I. S. Gradshteyn *et al.*, *Table of Integrals, Series, and Products*, 7th ed. New York, NY, USA: Academic, 2007.
[27] *Wolfram Mathematica Document*. Accessed: Nov. 25, 2021. [Online]. Available: http://functions.wolfram.com/06.06.21.0002.01

Lam-Thanh Tu was born in Ho Chi Minh City, Vietnam. He received the B.Sc. degree in electronics and telecommunications engineering from the Ho Chi Minh City University of Technology, Vietnam, in 2009, the M.Sc. degree in telecommunications engineering from the Posts and Telecommunications Institute of Technology, Vietnam, in 2014, and the Ph.D. degree from the Laboratory of Signals and Systems, Paris-Saclay University, Paris, France, in 2018. From 2015 to 2018, he was with the French National Center for Scientific Research (CNRS), Paris, as an Early Stage Researcher of the European-Funded Project H2020 ETN-5Gwireless. His research interests include stochastic geometry, LoRa networks, physical layer security, energy harvesting, and machine learning applications for wireless communications. He is currently a Research Fellow with the Xlim Research Institute, University of Poitiers, Poitiers, France. He was a recipient of the 2017 IEEE SigTelCom Best Paper Award. He was an Assistant Project Manager of the H2020 MCSA 5Gwireless and 5Gaura projects. He was an IEEE TRANSACTIONS ON COMMUNICATIONS Exemplary Reviewer in 2016.

Abbas Bradai (Senior Member, IEEE) received the Ph.D. degree from the LaBRI/University of Bordeaux, France, in 2012. He is an Associate Professor at the University of Poitiers and a Research Fellow at the XLIM Laboratory, Poitiers. His main research interests are multimedia communications over wired and wireless networks, cognitive radio, software-defined networks, and virtualization. He is/was involved in many French and European projects (ANR, FP7, and H2020), such as ENVISION, VITAL, and SAFE.

Yannis Pousset was born in 1971. He received the Ph.D. degree in mobile radio communication from the University of Poitiers in 1998. Since 2012, he has been a Professor at the Department of Electrical Engineering, University of Poitiers. He develops its research activities in the XLIM Laboratory. His research interests include the study of adaptive links related to the optimal transmission of data over wireless spatio-temporal radio channel.

Alexis I. Aravanis was born in Athens, Greece, in 1988. He received the Dipl.-Ing. (M.Sc. ECE) degree in electrical and computer engineering from the National Technical University of Athens (NTUA), Athens, in 2012, and the Ph.D. degree in telecommunications engineering from the Universitat Politècnica de Catalunya (UPC), Barcelona, Spain, seconded to the Centre National de la Recherche Scientifique (CNRS), Paris, France, under a Marie Curie ESR Fellowship, in 2019. Since 2020, he has been with the CentraleSupélec, where he is a Tenured Assistant Professor with the Laboratory of Signals and Systems (L2S) of CNRS, CentraleSupélec, and the University of Paris-Saclay, Paris. He has been the recipient of a Marie Curie ESR Fellowship in 2016 and is currently the recipient of a Marie Curie Individual Fellowship (IF) since 2020. He is a member of the Technical Chamber of Greece (TEE) and an Onassis Foundation Scholar. He serves as the Secretary for the RIS Emerging Technology Initiative of the IEEE Communications Society and of the RISE and REFLECTIONS Special Interest Groups of the IEEE Communications Society. He has served as the Managing Editor for IEEE COMMUNICATIONS LETTERS.